
ON THE POTENTIAL OF OPTIMAL TRANSPORT IN GEOSPATIAL DATA SCIENCE

Nina Wiedemann

Chair of Geoinformation Engineering
ETH Zürich
Switzerland
nwiedemann@ethz.ch

Théo Uscidda

CREST-ENSAE
Paris
France

Martin Raubal

Chair of Geoinformation Engineering
ETH Zürich
Switzerland

ABSTRACT

Prediction problems in geographic information science and transportation are frequently motivated by the possibility to enhance operational efficiency. Examples range from predicting car sharing demand for optimizing relocation to forecasting traffic congestion for navigation purposes. However, conventional accuracy metrics do not account for the spatial distribution of predictions errors, despite its relevance for operations. We put forward Optimal Transport (OT) as a spatial evaluation metric and loss function. The proposed OT metric assesses the utility of spatial prediction models in terms of the relocation costs caused by prediction errors. In experiments on real and synthetic data, we demonstrate that 1) the spatial distribution of the prediction errors is relevant in many applications and can be translated to real-world costs, 2) in contrast to other metrics, OT reflects these spatial costs, and 3) OT metrics improve comparability across spatial and temporal scales. Finally, we advocate for leveraging OT as a loss function in neural networks to improve the spatial correctness of predictions. This approach not only aligns evaluation in GeoAI with operational considerations, but also signifies a step forward in refining predictions within geospatial applications. To facilitate the adoption of OT in GIS, we provide code and tutorials at <https://github.com/mie-lab/geospatialOT>.

Keywords GeoAI · spatio-temporal modelling · Earth Mover’s Distance · evaluation framework

1 Introduction

Geographic Information Science (GIS) aims to develop analysis and prediction tools tailored to the specific challenges involved with geographic data, true to the mantra “spatial is special”. Meanwhile, the vast majority of GeoAI research aims to implement a spatially-explicit *model design* [46, 40, 63], while spatial considerations in the *model evaluation* are neglected. Consider the following examples: In weather forecasting, locating a rain shower 50km from its actual occurrence is clearly worse than mislocating it by 5km. In bike or car sharing demand prediction, underestimating demand at a station forces users to relocate to other stations, leading to longer relocation times if high supply is allocated far from areas of high demand. Local deviations in traffic forecasts are less severe than an occurrence of traffic congestion far from the expected location. Last, errors in predicting wildfire spread involve costly re-allocation of firefighting resources, which are the more time-consuming the farther the predicted direction of fire spread is from its real direction. In sum, the *spatial distribution* of prediction errors plays an important role for many applications in GIS and transportation, and evaluation frameworks should account for the costs arising from relocation or resource allocation effort.

Currently, GeoAI methods are evaluated with standard error metrics such as the mean squared error (MSE) or mean absolute percentage error (MAPE) [42, 7, 92, 65]. These metrics average the error over locations, ignoring the impact of

prediction errors on downstream tasks such as bike relocation, traffic management, or mission planning for firefighting. Consequently, there is a mismatch between how predictions are evaluated and their practical utility. This issue has been previously noted in transportation research [111]; yet, there is a lack of work to close this gap. Precisely quantifying the utility of predictive models would require deploying them in real-world applications or simulations, and measuring their utility, e.g. in terms of relocation costs or user satisfaction. For instance, Peled et al. [70] analyze how the optimized performance of a public transport fleet changes with the noise level of the predictions. On the other hand, application-independent measures of the errors' spatial distribution exist in the field of spatial statistics, e.g. in the form of indicators for spatial autocorrelation. These methods allow to identify clusters of over- or underestimation and have been used to evaluate a model's ability to account for spatial heterogeneity [115, 16]. However, they cannot measure relocation or resource allocation costs and lack interpretability and robustness towards their parameters [19].

In this work, we propose to evaluate spatial prediction models with Optimal Transport (OT). OT is a mathematical framework providing methods to measure the disparity between two distributions. Within GIS, OT primarily appears in the form of the Earth Mover's Distance (EMD). Here, we show how OT can be leveraged to compare the real and predicted spatial distributions in geospatial applications. As illustrated in Figure 1, the proposed OT metric measures the *spatial costs* of prediction errors in terms of the redistribution effort necessary to align the predictions with the ground truth. In contrast, standard metrics such as the mean squared error (MSE) treat all locations independently and cannot account for spatial costs. Crucially, OT is not limited to Euclidean distances, but can reflect application-specific and interpretable costs such as user relocation time or monetary costs for resource reallocation. Our framework is based on partial OT [36, 74, 66] and is applicable to any spatio-temporal prediction task, such as estimating bike sharing demand, traffic congestion, charging station occupancy, wildfire spread or deforestation rates (see Table 1).

Our contribution is two-fold: On the one hand, we introduce a new evaluation framework to GeoAI, discussing its relevance in various geospatial applications, demonstrating its ability to reflect real-world costs, its relation to spatial autocorrelation, and its potential for comparing different spatial and temporal scales. On the other hand, we enable OT as a loss function to train GeoAI models, and present experiments where training with an OT loss effectively reduces spatial costs.

The remainder of the paper is structured as follows: In section 2, we introduce OT-based metrics for spatio-temporal predictions, positioning our work within the broader context of OT and GeoAI research. In section 3 we empirically illustrate the potential of OT as an *evaluation* framework in GIS, and section 4 presents experiments using this novel metric as a *loss* function. Finally, we discuss challenges and limitations of applying OT in section 5 and present conclusions in section 6.

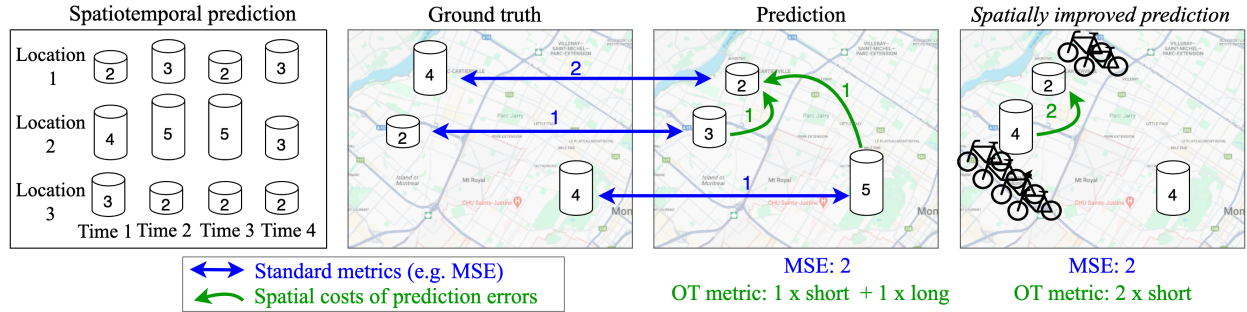


Figure 1: Optimal transport as an evaluation framework in geospatial data science. Spatio-temporal prediction problems involve forecasting spatial observations over time, such as estimating bike-sharing demand at multiple stations (left). Conventional metrics usually treat locations independently, ignoring their spatial distribution (blue). In contrast, our Optimal Transport (OT) framework accounts for spatial costs, quantifying prediction errors in terms of the effort required for relocation or resource allocation, such as relocating bicycles between stations (green).

Application	Category	Relevance	Locations	Spatial costs	Interpretation
Wildfire spread prediction	Vision-based GeoAI	Improve resource allocation for firefighting	Cells in geographic raster data	Operational costs for relocating resources between cells	Resource reallocation costs (distance between predicted and true fire spread)
Weather forecasting	Vision-based GeoAI	Adequate preparation and planning	Cells in geographic raster data	Euclidean distance	OT error indicates spatial displacement of an occurring weather phenomenon wrt. the prediction
Bike, scooter or car sharing demand prediction	Spatiotemporal time series forecasting	Efficient allocation of supply	Stations of shared system	Map-matched driving distances (relocation costs)	Costs for resources re-allocations or for users to relocate due to prediction errors
EV charging station occupancy prediction	Spatiotemporal time series forecasting	Supporting navigation	EV charging stations	Map-matched driving distance	Opportunity costs for drivers to relocate due to prediction errors
Deforestation rate estimation	Spatial interpolation	Inform policy and intervention measures by identifying areas at high risk of deforestation	Towns or regions	Communication distance between places	OT error indicates spatial mismatch between potential intervention measures and actual deforestation
Estimation of heavy metal pollution	Spatial interpolation	Monitoring and intervention against pollution	Measurement locations	Euclidean distance	Spatial displacement of pollution estimates & opportunity costs

Table 1: Potential applications for spatial evaluation metrics, such as the OT distance. Spatial costs are defined between locations in the form of raster cells, points or regions. The user-defined cost matrix allows for an application-specific interpretation of the spatial prediction error, e.g. as relocation costs, resource allocation or opportunity costs. In [subsection 3.2](#), we showcase the framework using real bike sharing data.

2 Methods: Optimal Transport metrics for spatiotemporal predictions

2.1 The Optimal Transport framework

By providing a simple and comprehensive framework to compare probability distributions, optimal transport (OT) theory [84] has inspired many developments in machine learning [72]. The scope of its applications has now reached several fields of science such as single-cell biology [88, 112, 8, 26, 52, 49], imaging [89, 38, 33, 25], neuroscience [45, 44, 55, 99], or, naturally, economics [31] which was the initial source of inspiration for the field. Additionally, a flurry of works have recently connected it to other trending topics, such as convex neural networks [67, 54, 41, 106], normalizing flows [101, 59, 76, 103, 102, 53, 27], diffusion models [24, 91, 6, 60, 61], attention mechanisms [83, 98], or disentangled representational learning [69, 107].

Solving an OT problem involves finding the most cost-effective way to transport a source distribution μ to a target distribution ν . Focusing here on discrete distributions, let $\mu = \sum_{i=1}^n \mathbf{p}_i \delta_{\mathbf{x}_i}$ and $\nu = \sum_{j=1}^m \mathbf{q}_j \delta_{\mathbf{y}_j}$, where $\mathbf{p} = (\mathbf{p}_1, \dots, \mathbf{p}_n)$ and $\mathbf{q} = (\mathbf{q}_1, \dots, \mathbf{q}_m)$ are histograms and $\mathbf{x}_1, \dots, \mathbf{x}_n$ and $\mathbf{y}_1, \dots, \mathbf{y}_m$ are the locations in \mathbb{R}^d where the mass of each measure lies. Additionally, let $c : \mathbb{R}^d \times \mathbb{R}^d \rightarrow \mathbb{R}$ be a cost function, s.t. $c(\mathbf{x}, \mathbf{y})$ measures the cost of moving a unit of mass from location \mathbf{x} to location \mathbf{y} . Our goal is to transport μ onto ν through a coupling matrix $\mathbf{T} \in \mathcal{U}(\mathbf{p}, \mathbf{q}) := \{\mathbf{T} \in \mathbb{R}_+^{n \times m} \mid \mathbf{T} \mathbf{1}_n = \mathbf{p}, \mathbf{T}^\top \mathbf{1}_m = \mathbf{q}\}$ while minimizing the cost of transportation quantified by c . Here, \mathbf{T}_{ij} denotes the amount of mass transported from \mathbf{x}_i to \mathbf{y}_j . In other words, given the matrix $\mathbf{C} := [c(\mathbf{x}_i, \mathbf{y}_j)]_{1 \leq i, j \leq n, m} \in \mathbb{R}^{n \times m}$ containing the pairwise cost of transport between the locations of the support of μ and ν , we want to solve the following optimization problem:

$$\min_{\mathbf{T} \in \mathcal{U}(\mathbf{p}, \mathbf{q})} \sum_{i,j=1}^{n,m} \mathbf{T}_{ij} \mathbf{C}_{ij} \Leftrightarrow \min_{\mathbf{T} \in \mathcal{U}(\mathbf{p}, \mathbf{q})} \langle \mathbf{T}, \mathbf{C} \rangle \quad (1)$$

where $\langle \cdot, \cdot \rangle$ denotes the Frobenius inner product. The OT problem (1) is a linear program, which can be solved using, e.g., the network-simplex algorithm [5]. We call any solution \mathbf{T}^* to this problem, which always exists, an OT coupling. Through the optimal transportation cost provided by \mathbf{T}^* , we define the c -Wasserstein distance:

$$W_c(\mu, \nu) = \min_{\mathbf{T} \in \mathcal{U}(\mathbf{p}, \mathbf{q})} \langle \mathbf{T}, \mathbf{C} \rangle = \sum_{i,j=1}^{n,m} \mathbf{T}_{ij}^* \mathbf{C}_{ij}. \quad (2)$$

This quantity is also referred to as the Earth Mover’s Distance (EMD) [81]. When $c(\mathbf{x}, \mathbf{y}) = \|\mathbf{x} - \mathbf{y}\|_2^q$ for any $p \geq 1$, $W_c(\mu, \nu) = 0$ i.f.f. $\mu = \nu$ [84, Prop. 5.1]. As a result, W_c provides a natural quantity to compare distributions. This plays a fundamental role in our approach.

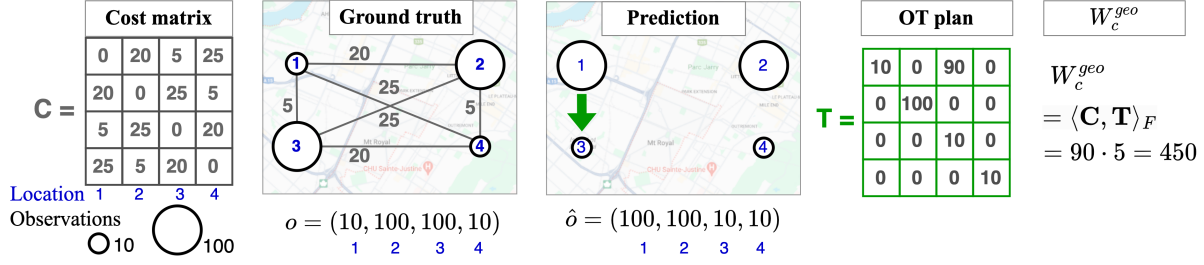


Figure 2: Quantifying spatial costs with Optimal Transport. Given a cost matrix C defined between location pairs, prediction errors are measured in terms of the minimal transport costs required to align the predictions with the true observations (see subsection 2.2). In the example, a mass of 90 must be transported from location 1 to location 3 with cost 5, leading to an OT error of 450.

2.2 Optimal Transport for evaluating spatiotemporal predictions

In this work, we investigate the use of this distance as an evaluation metric and loss function for geospatial forecasting challenges. Assume that a GeoAI model provides predictions at fixed locations, such as pickups at bike sharing stations (see Figure 1). To repurpose OT for spatial evaluation, we proposed to set μ to the predicted and ν to the true spatial distribution of observations. This approach utilizes the Wasserstein distance between *signatures*, a special case where both distributions are defined over the same locations ($n = m$ and $\mathbf{x}_i = \mathbf{y}_i$, $\forall i \in \{1, \dots, n\}$), but with different histograms. Let $\mathbf{x}_1, \dots, \mathbf{x}_n$ be the spatial locations, and let $\mathbf{o} = (\mathbf{o}_1, \dots, \mathbf{o}_n)$ be the true observations and $\hat{\mathbf{o}} = (\hat{\mathbf{o}}_1, \dots, \hat{\mathbf{o}}_n)$ the predicted observations at these locations. Thus, the source and target distribution (μ and ν) are set to the predicted spatial observations, $\mu = \sum_{i=1}^n \hat{\mathbf{o}}_i \delta_{\mathbf{x}_i}$, and the true observations $\nu = \sum_{i=1}^n \mathbf{o}_i \delta_{\mathbf{x}_i}$. For instance, \mathbf{o}_i could represent the demand for shared bicycles at the i -th bike sharing station, located at \mathbf{x}_i . For geospatial data, the locations \mathbf{x} are usually two-dimensional, $\mathbf{x} \in \mathbb{R}^2$.

By selecting an appropriate cost function c between locations and setting $C_{ij} = c(\mathbf{x}_i, \mathbf{x}_j)$, we can solve Problem (1) between μ and ν to compute $W_c(\mu, \nu)$. In sum, we define the cost-dependent geospatial OT error as

$$W_c^{geo} = W_c(\mu, \nu) \text{ with } \mu = \sum_{i=1}^n \hat{\mathbf{o}}_i \delta_{\mathbf{x}_i}, \nu = \sum_{i=1}^n \mathbf{o}_i \delta_{\mathbf{x}_i} \quad (3)$$

This value represents the minimal transportation cost required to redistribute the mass from μ to match the distribution in ν , and translates to the minimal cost necessary to align the predicted with the true spatial distribution of observations. In other words, we propose to regard $W_c^{geo}(\mu, \nu)$ as a metric for the spatial goodness of a prediction, as $W_c^{geo}(\mu, \nu)$ measures the total spatial costs to “undo” errors of the predictive model.

Figure 2 provides an example, where the cost was set to a symmetric matrix with low spatial cost C_{13} between locations 1 and 3, due to their short distance. The prediction error, here an overestimation of \mathbf{o}_1 and underestimation of \mathbf{o}_3 , results in transportation costs of 90 between location 1 and 3 ($T_{13} = 90$), while no transport is necessary for the other locations. The total costs are thus $W_c^{geo} = \sum_{i,j=1}^{n,m} T_{ij}^* C_{ij} = 90 \cdot C_{13} = 450$. In general, suitable cost functions may include the Euclidean distance (or another p -norm-between locations), monetary costs, map-matched driving distances, or CO₂ emissions. If the cost matrix corresponds to the (squared) Euclidean distance between the locations defined by two-dimensional geographic coordinates, i.e., $C_{ij} = c(\mathbf{x}_i, \mathbf{x}_j) = \|\mathbf{x}_i - \mathbf{x}_j\|_2^2$, this corresponds to the 2-Wasserstein distance, $W_2^2(\mu, \nu)$.

While we have focused on spatial predictions with *fixed* locations, it is important to note that the metric can be easily extended to applications where the predicted locations differ from the locations of the true observations ($n \neq m$ and $\mathbf{x}_i \neq \mathbf{y}_i$). An example of this is provided in Appendix B, where we predict the locations of high deforestation risk and measure the spatial error of these predictions using OT.

2.3 Partial Optimal Transport

The standard formulation of OT, balanced OT, as introduced above, assumes the total mass of both distributions to be equal, which is unlikely in our application unless the observations are normalized. A variant of OT that allows for differences between the total masses is called Unbalanced Optimal Transport and was already introduced by Kantorovich and Rubinshtein [47]. The latest research on Unbalanced OT commonly employs a static formulation that relaxes the marginal constraints in Problem 1 and instead just minimizes the divergence between the distributions and the marginals

of the transportation plan [15, 18, 58, 90, 73]. However, this formulation is unsuitable for geospatial applications due to its lack of interpretability. Since the constraints are relaxed, the transportation matrix is not executable in practice, and the resulting total cost cannot distinguish between distribution-induced costs (costs according to the balanced OT formulation) and costs that are due to the overall mass-mismatch. Another stream of work proposes *partial OT*, which deals with mass imbalance by posing an explicit costs on the discarded mass that cannot be coupled. In partial OT, so-called “dummy points” [14], “dustbin” [86, 22] or “waste vectors” [36] are added, allowing mass to vanish or to emerge with a certain cost; here denoted ϕ . While this approach is more suitable for our purposes, its general formulation requires that only a fraction of the mass is transported. Instead, we aim to transport as much mass as possible, since all prediction errors should optimally be balanced out by inter-location transport. The maximum mass to be transported is either the total mass of the source or of the target distribution, $\min(\sum_{i=1}^n \mathbf{o}_i, \sum_{i=1}^n \hat{\mathbf{o}}_i)$. This boils down to a special case of the formulation of Chapel et al. [14], who show that the problem can be reduced to the standard OT formulation by extending the measures and the cost matrix.

Following Chapel et al. [14], we add a dummy location \mathbf{x}_{n+1} in both source and target distribution. The mass at this dummy point is set to zero or the total mass difference ($|\sum_{i=1}^n \mathbf{o}_i - \sum_{i=1}^n \hat{\mathbf{o}}_i|$) respectively, dependent on whether the source or target distribution has larger mass. Formally, let $s = \min(\sum_{i=1}^n \mathbf{o}_i, \sum_{i=1}^n \hat{\mathbf{o}}_i)$, and we define $\mathbf{o}_{n+1} = \sum_{i=0}^n \hat{\mathbf{o}}_i - s$, and $\hat{\mathbf{o}}_{n+1} = \sum_{i=0}^n \mathbf{o}_i - s$. For example, if the true bike sharing demand over all locations is 10 ($\sum_{i=1}^n \mathbf{o}_i = 10$), and the predicted total demand is 12, we add a dummy location with $\mathbf{o}_{n+1} = 2$ and $\hat{\mathbf{o}}_{n+1} = 0$. We denote the adapted measures including the dummy points as $\tilde{\mu}$ and $\tilde{\nu}$, which now have equal mass by design.

Furthermore, the cost matrix is adapted accordingly, penalizing the overshooting mass with a fixed cost of ϕ :

$$\tilde{\mathbf{C}}(\phi) = \begin{pmatrix} c_{11} & \dots & c_{1n} & \phi \\ \dots & \ddots & \dots & \dots \\ c_{n1} & \dots & c_{nn} & \phi \\ \phi & \dots & \phi & \phi \end{pmatrix} \quad (4)$$

$$(5)$$

As Chapel et al. [14] show, the exact solution for OT can be computed simply by applying balanced OT on $\tilde{\mu}, \tilde{\nu}$ and $\tilde{\mathbf{C}}$. Thus, we define the geospatial partial OT error, subject to ϕ , as

$$W_{c,\phi}^{geo} = W_{\tilde{\mathbf{C}}}(\tilde{\mu}, \tilde{\nu}) \text{ with } \tilde{\mu} = \sum_{i=1}^{n+1} \hat{\mathbf{o}}_i \delta_{\mathbf{x}_i}, \tilde{\nu} = \sum_{i=1}^{n+1} \mathbf{o}_i \delta_{\mathbf{x}_i} \quad (6)$$

The solution yields a transportation matrix that contains the flow of mass between locations, as well as the outflow or inflow dependent on the total mass difference. In our evaluation framework, $W_{c,\phi}^{geo}$ can be seen as a combination of the total error over all locations, $\sum_{i=1}^n \mathbf{o}_i - \sum_{i=1}^n \hat{\mathbf{o}}_i$, and the distributional error due to the spatial costs between locations. The larger ϕ , the larger the part of $W_{c,\phi}^{geo}$ expressing the total prediction error. The smaller ϕ , the more focus lies on the distributional errors. It is worth noting that the penalty ϕ could easily be defined in a location-dependent manner; i.e., penalizing the import / export to some locations more than to others. For instance, this could be useful when considering predictions of bike sharing demand, where bikes are transported from one distribution center to the stations.

2.4 Related work

While OT has become a popular tool in other applied fields such as computational biology [87, 8, 9, 12, 10, 53], there is very limited work in the context of GeoAI, despite the roots of OT in transportation research. There are few exceptions; for example, Roberts et al. [80] experiment with spatiotemporal predictions in their methodological work on Gini-regularized OT. Janati et al. [45] propose OT as a measure for the similarity of spatial time series with applications for clustering. Liu et al. [64] coin the term “geographical optimal transport” for their application of OT for relocating geotagged tweets based on remote sensing data. More related work can be found in the realm of shared transport services, due to the obvious connection between OT and relocation. For example, Treleaven and Frazzoli [104], Treleaven et al. [105] employ the EMD with a road-map-based cost matrix for optimizing relocation in one-way car sharing, and Qian et al. [77] measure the distance between bike sharing and public transport stations with the EMD. One form of unbalanced OT was proposed under the term “graph-based equilibrium metric” [116] for measuring supply-demand discrepancies in ride sharing, with follow-up work that extends the metric by a more supply-sided view [17].

However, besides the general scarcity of OT in GeoAI, to the best of our knowledge, there is no general analysis on using OT for evaluating spatiotemporal predictions. We fill this gap with the presented framework and an in-depth analysis of the benefits and opportunities of OT in Spatial Data Science provided in the following section.

3 OT as an evaluation framework: Relevance, spatial relations, and scaling properties

Our rationale for introducing a new evaluation framework in GeoAI is three-fold: 1) In comparison to existing metrics, OT is *spatially-explicit* and extends existing evaluation frameworks, 2) spatial errors are interpretable and *relevant* for a wide range of GeoAI applications, and 3) OT errors enable *comparability across scales*, as well as across space and time. In the following sections, we will successively explain these arguments, supported by empirical evidence from experiments on real and synthetic geospatial data.

3.1 OT in relation to other metrics

To highlight the benefits of our proposed OT evaluation framework, we compare OT errors to the MSE as a standard error metric. We use synthetic data to demonstrate empirically that OT captures fundamentally different costs than the MSE, and relate these differences to spatial autocorrelation, a core concept in GIS.

3.1.1 Comparison to the mean squared error

A synthetic scenario is designed to allow to systematically vary the spatial costs. Intuitively, the spatial costs, i.e. the transport costs to align ground truth and predictions, are higher if the residuals are unevenly distributed in space. To construct a simple scenario accordingly, we sample residuals from different distributions dependent on the x-coordinate of their location. Let $\mathbf{x}_{i,1}$ denote the first component of the location vector, i.e., its x-coordinate, and $\mathbf{x}_{i,2}$ the y-coordinate. The locations ($n = 100$) are randomly sampled from a uniform distribution $\mathbf{x}_{i,1}, \mathbf{x}_{i,2} \sim U[0, 100] \quad \forall i$, and the residuals from $\mathcal{N}(\mu, \sigma)$ for all locations with $\mathbf{x}_{i,1} < 50$ and $\mathcal{N}(-\mu, \sigma)$ for $\mathbf{x}_{i,1} \geq 50$. The higher the μ , the larger the *spatial imbalance* of the residuals, i.e., the difference between the residuals at $\mathbf{x}_{i,1} < 50$ and the ones at $\mathbf{x}_{i,1} \geq 50$. Figure 3 provides two examples, with $\mu = 0$ corresponding to evenly distributed residuals, whereas $\mu = 1.5$ results in an unbalanced spatial distribution. Such imbalance is very common in geospatial data due to spatial autocorrelation and spatial heterogeneity [115].

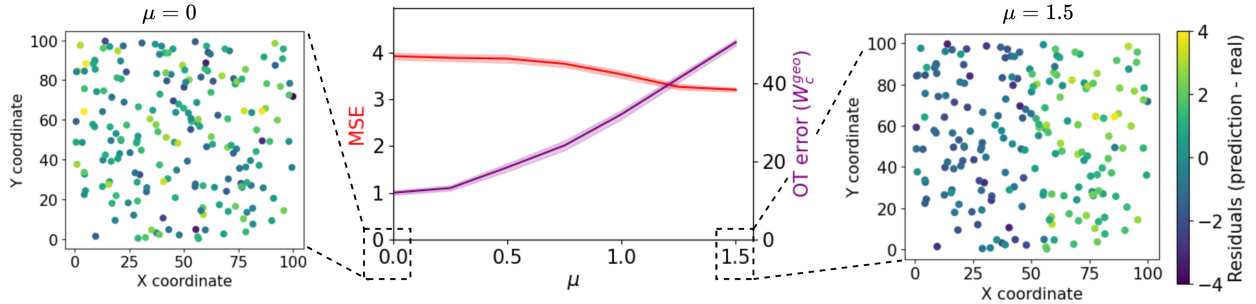


Figure 3: Comparison of MSE and OT error on synthetic data with increasingly unbalanced residuals ($\mu = 0$: no imbalance, $\mu = 1.5$: strong spatial imbalance). The imbalanced residuals lead to larger spatial costs, which is evident from the increasing OT error. There is also an evident relation of OT to spatial autocorrelation.

Figure 3 illustrates the OT error and the MSE for $\mu \in \{0, 0.5, 1, 1.5\}$. σ was tuned to keep the average absolute value of the residuals constant. While the MSE remains constant, the OT error increases with the spatial imbalance, reflecting the increased transportation costs if the residuals are clustered in space, corresponding to large areas of oversupply distinct from areas of high demand. In turn, the transportation costs are lower if the errors are distributed randomly, since neighboring errors offset one another.

3.1.2 Relation to spatial autocorrelation of the residuals

The synthetic experiment in Figure 3 shows that OT costs are higher if the residuals are clustered in space. This observation indicates a relation between OT and spatial autocorrelation. There are several measures to quantify spatial autocorrelation in a dataset, with global Moran's I [68] arguably the most popular one. Moran's I is defined as:

$$I = \frac{n}{\sum_{i,j=1}^n \mathbf{w}_{ij}} \cdot \frac{\sum_{i,j=1}^n \mathbf{w}_{ij} (\mathbf{v}_i - \bar{\mathbf{v}})(\mathbf{v}_j - \bar{\mathbf{v}})}{\sum_{i=1}^n (\mathbf{v}_i - \bar{\mathbf{v}})^2} \quad (7)$$

where \mathbf{v}_i is the observation at the i -th location, $\bar{\mathbf{v}}$ is the mean of all observed values, n is the number of locations, and \mathbf{w}_{ij} is the (distance-based) weighting between two points.

We empirically confirm the observed relation between the OT error and spatial autocorrelation by computing Moran's I on the synthetic data generated in [subsection 3.1](#). For maximal comparability, we set the weights \mathbf{w}_{ij} to the negative costs, $\mathbf{w}_{ij} = -\mathbf{C}_{ij}$. Indeed, [Figure 4](#) testifies a strong correlation of Moran's I and the OT loss ($r = 0.98$), largely independent from the MSE.

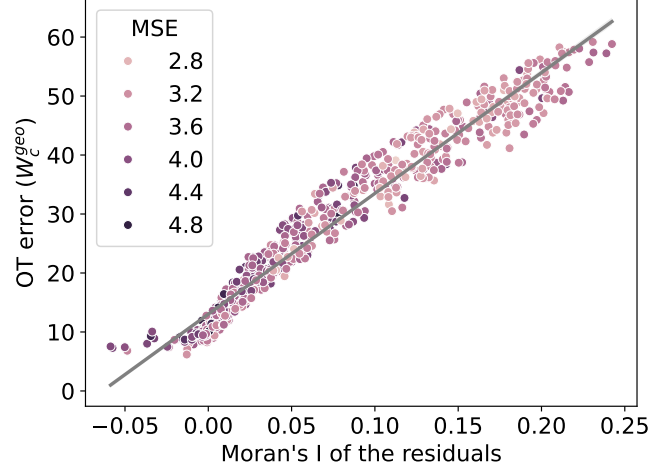


Figure 4: Correlation of the OT error with the spatial autocorrelation of the residuals. Spatial autocorrelation is measured with Moran's I. Each point corresponds to the predictions for all locations at a specific time. The OT error strongly correlates with Moran's I, rather independent of the MSE.

To understand this relation further, we examine the formula for Moran's I. We plug the residuals into [Equation 7](#) by setting $\mathbf{v}_i = \mathbf{o}_i - \hat{\mathbf{o}}_i$. To simplify I , we further assume *balanced* OT, with $\sum_{i=1}^n \mathbf{o}_i = \sum_{i=1}^n \hat{\mathbf{o}}_i$. It follows that

$$\bar{\mathbf{v}} = \frac{1}{n} \sum_{i=1}^n \mathbf{v}_i = \frac{1}{n} \sum_{i=1}^n (\mathbf{o}_i - \hat{\mathbf{o}}_i) = \frac{1}{n} \sum_{i=1}^n \mathbf{o}_i - \frac{1}{n} \sum_{i=1}^n \hat{\mathbf{o}}_i = 0 \quad (8)$$

Thus, Moran's I of the residuals becomes

$$I_{residuals} = \frac{n}{\sum_{i,j=1}^n \mathbf{w}_{ij}} \frac{\sum_{i,j=1}^n \mathbf{w}_{ij} (\mathbf{o}_i - \hat{\mathbf{o}}_i) (\mathbf{o}_j - \hat{\mathbf{o}}_j)}{\sum_i (\mathbf{o}_i - \hat{\mathbf{o}}_i)^2} \quad (9)$$

Furthermore, we can express the weights \mathbf{w}_{ij} in terms of costs by setting $\mathbf{w}_{ij} = -\mathbf{C}_{ij}$. The normalization factor $n / \sum_{i,j=1}^n \mathbf{w}_{ij}$ can be dropped as the cost matrix and the number of location is constant. These changes result in:

$$I_{simplified} = \frac{\sum_{i,j=1}^n -\mathbf{C}_{ij} (\mathbf{o}_i - \hat{\mathbf{o}}_i) (\mathbf{o}_j - \hat{\mathbf{o}}_j)}{\sum_{i=1}^n (\mathbf{o}_i - \hat{\mathbf{o}}_i)^2} \quad (10)$$

While there is no direct theoretical relation between both measures ([Equation 10](#) and [Equation 3](#)), the definition allows to understand their commonalities and differences. High OT errors, as well as high Moran's I, arise from low spatial distance between residuals of similar value, and large distance between residuals of differing value. While Moran's I focuses more on the relation between *nearby* points, the OT error is driven by the values of *distant* points. Furthermore, OT provides an explicit *coupling* of residuals by computing the transport plan, whereas Moran's I measures the general spatial patterns of the residuals.

Thus, OT translates the rough indication of the spatial distribution of the residuals, provided by Moran's I, into a more precise measure of the associated operational costs. Although OT cannot replace Moran's I or other measures for spatial autocorrelation, it provides a way to merge spatial considerations into standard error metrics for spatio-temporal data. For instance, it can help to uncover spatial heterogeneity in the data. More generally speaking, the close link between OT and such a fundamental GIS concept as Moran's I supports the value of OT in GIS.

3.2 Interpretability and relevance of spatial errors

The OT error provides a highly interpretable measure of the costs associated with prediction errors, especially those with spatial autocorrelation. As shown in Table 1 and further explained in Appendix A, the interpretation of the OT error depends on the application and on the definition of the cost matrix \mathbf{C} . It could, for example, represent the total relocation distance, resource allocation costs, or opportunity costs. Such flexibility makes OT applicable to a wide range of applications, including raster-based GeoAI (e.g. land use classification [2], glacier retreat prediction, weather forecasting [48], or wildfire spread prediction [79, 82]), point-data spatio-temporal time series (e.g. mobility demand prediction [93, 42, 113, 78, 62, 57, 117, 1, 109]), or even spatial interpolation (e.g. inferring heavy metal pollution [28]).

In the following, we utilize bike sharing demand prediction as a running example to demonstrate the properties of OT on real-world data. A public dataset is available from the BIXI bike sharing service in Montreal. The number of bike pickups at 458 stations is aggregated by hour and by station, following Hulot et al. [42]. A state-of-the-art time series prediction model, N-HiTS [13], is trained to predict the demand for the next five hours at any time point. The predictions are evaluated on a hundred time points from the test data period. For details on data preprocessing and model training, see Appendix C and Appendix D respectively.

3.2.1 Case study: Relocation costs in bike sharing demand prediction

First, we demonstrate the computation of the OT error using one example of bike-sharing demand predictions, for a single point in time. For visualization purposes, we subsample one third of the stations. Figure 5 shows the spatial distribution of the residuals at these stations, highlighting, for example, a few stations with significantly underestimated demand (big purple circles) or an overestimation of bike-sharing demand in the bottom-left (orange points). Calculating the OT error involves computing \mathbf{T}^* , the optimal transport matrix. We apply partial OT with $\phi = 0$, essentially computing the difference between both distributions without penalizing the total difference of their masses (see subsection 2.3). The arrows in Figure 5 illustrate all nonzero cells of \mathbf{T}^* , representing all required redistribution of mass to align the predictions with the true observations. The length of the arrows corresponds to the transport cost, since \mathbf{C} was set to the Euclidean distance between stations. In this example, most errors can be balanced out between neighboring stations, resulting in mass being relocated over short distances from prediction to ground truth. It is worth noting that a few errors are not balanced out since they are ignored through partial OT (see orange point in the bottom-left). The total spatial error corresponds to the sum of all arrow lengths when $\phi = 0$, here $W_{c,0}^{geo} = \sum_{i,j=1}^n \tilde{\mathbf{C}}_{ij} \mathbf{T}_{ij}^* = 34.85$.

To interpret this error, assume that relocating one bicycle over one kilometer costs \$5. $W_{c,0}^{geo}$ represents the total relocation kilometers required to match the real bike-sharing demand with the predicted supply (apart from their total difference). Thus, the error of this prediction model would cost the bike-sharing service $34.85 \cdot \$5 = \174.25 if they needed to fully rebalance their supply to meet future demand. The OT framework’s output could be integrated into more complex analysis tools specific to the company, such as considering the option of collecting and redistributing multiple bicycles simultaneously.

3.2.2 Flexibility to define application-specific cost matrices

A major strength of OT is its flexibility to incorporate any arbitrary cost function, without requirements on the function’s smoothness or other properties. This enables tailored application-specific analyses. In the bike sharing example, we could also interpret prediction errors as *users* having to walk from one station to another. In this case, it is more sensible to set \mathbf{C} to map-matched walking distances. On top of that, the effort of users is not linear, since users would dismiss bike sharing as a transport option when no bike is available in any feasible distance. We construct a cost matrix accordingly, where the cost between pairs of locations that are closer than 2km corresponds to the map-matched walking distance, and the cost between all other pairs is set to 15km to express the high costs of losing customers when no bike is available anywhere nearby. Figure 6c provides the new cost matrix in comparison to a simple Euclidean-distance based matrix, and shows the resulting OT errors $W_{c,0}^{geo}$ for the test set, i.e., the predictions from the N-HiTS model for 100 randomly selected time points. The errors correlate, but the map-matched cost matrix generally results in larger relocation costs and very different results for certain samples.

3.2.3 Relation to MSE and Moran’s I for real data

To investigate the observations from subsection 3.1 on real data, we compute the MSE, the OT error and Moran’s I for the bike sharing data on the test set. We expect the MSE to correlate with the OT error for real data, since a larger MSE typically goes along with greater mass redistribution. Figure 7 confirms this intuition, showing a Pearson correlation of $r = 0.38$ between the MSE and W_c^{geo} (with $\phi = 0$). Similarly, there is a weak correlation between the OT error and Moran’s I ($r = 0.2$). The reasons for this weaker correlation, compared to the synthetic dataset (Figure 4), are 1) the

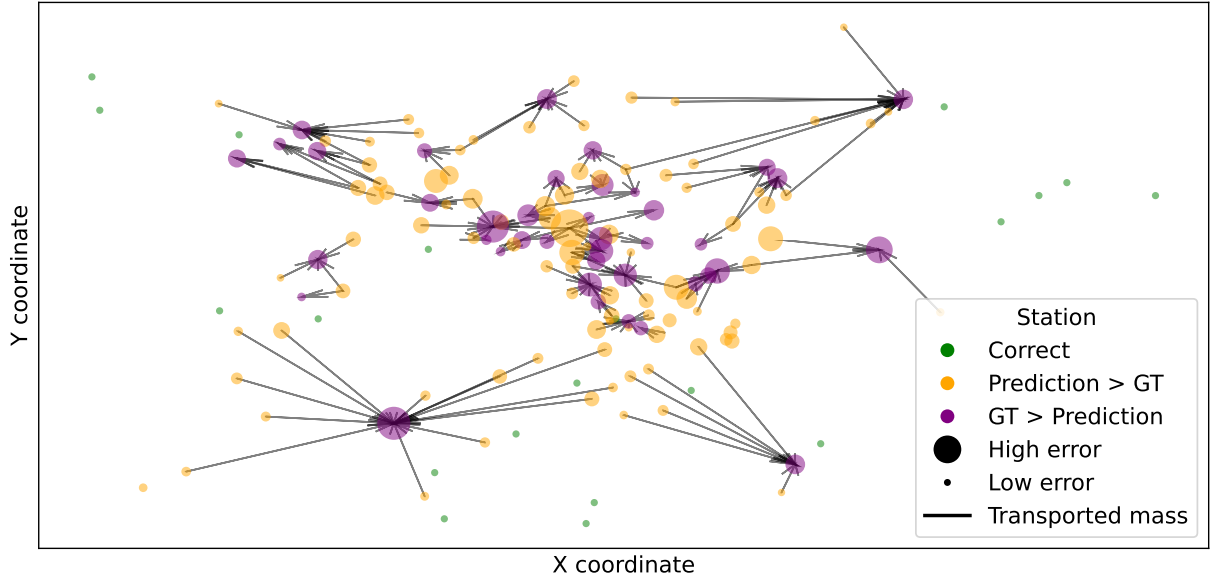


Figure 5: Transport map as computed with the OT framework. The goodness of the prediction is measured in terms of the relocation costs necessary to align the predictions with the real observations. Here, the difference between real and predicted bike sharing demand is shown, where mass is transported from bike sharing stations with overestimated demand (orange) to stations where the demand was underestimated (purple). In the example, the total spatial costs are rather low since most errors are balanced out with nearby points.

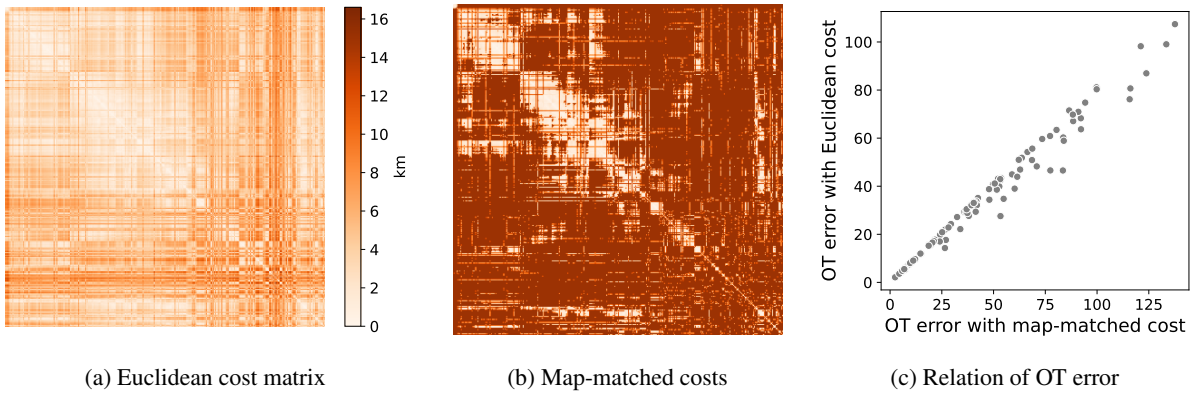


Figure 6: Dependence of the OT error on the given cost matrix. Our OT-based evaluation framework can incorporate application-dependent cost matrices. For example, a map-matched cost matrix (with cutoff) leads to larger errors than a simple Euclidean-distance-based cost matrix.

interdependence with the MSE, 2) the generally low spatial autocorrelation in the bike sharing data, 3) the low variance of the spatial autocorrelation in the data, which was controlled for the synthetic data. Together, MSE and Moran’s I explain 58% of the variance of the OT error when fitting a linear model, with coefficients of 1.04 and 0.93, respectively. This demonstrates that OT combines both components into a unified metric while adding unique properties on top, by considering relocation distances explicitly.

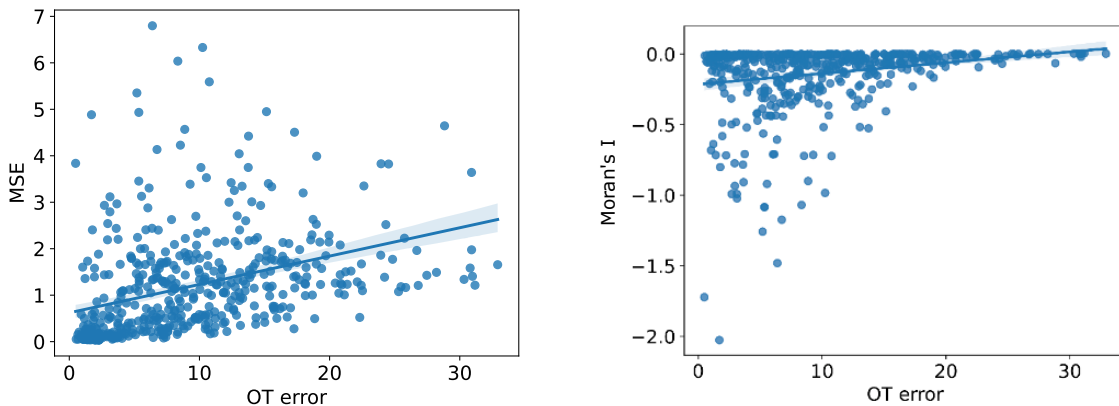


Figure 7: Relation between the OT error, the MSE and Moran’s I for bike sharing data. Each point represents the metric value for evaluating the predictions at all locations for one time point. The OT evaluation metric relates to the MSE but at the same time measures other phenomena. The spatial autocorrelation is generally low, also correlating weakly with the OT error.

3.3 Comparability across scales

Research on spatio-temporal data frequently resorts to aggregating data across both space and time, leading to incomparable outcomes due to the Modifiable Areal Unit Problem (MAUP). Already in 1934, Gehlke and Biehl [34] noticed that the size and grouping of census tract areas changes the correlation coefficient of the analyzed variables; an effect that was later related to spatial heterogeneity [30]. Since then, the MAUP was evidenced in numerous geospatial applications [11], including mobility data [110, 32, 97]. While most research on the topic describes the effect on *analysis* results, the MAUP was also shown to affect spatio-temporal *predictions*, e.g., in traffic forecasting [114] or next location prediction [96, 95, 20].

In the realm of time series analysis, Hyndman et al. [43] have made significant strides in addressing this concern through their concept of hierarchical reconciliation [4, 71]. Their approach regards general cross-sectional groupings of time series, not limited to but including spatial groupings, and they propose methodologies to generate forecasts consistent across the scale hierarchy [108]. Hierarchical reconciliation was shown to improve prediction accuracy in applications such as traffic forecasting [51] and can be extended to providing consistency across space *and* time [56]. Nonetheless, their framework achieves consistency but not comparability across scales, and falls short in accounting for fuzzy groupings that arise from the ambiguity of clustering spatial locations.

3.3.1 Spatial aggregation scales and the MAUP

We argue that OT allows to compare results across scales and between different aggregation methods. Intuitively, aggregating the data in space decreases the error, since the clustered observations are less noisy, but the *utility* of the predictions is lower when they are not available on a fine-grained per-location level. In the following, we demonstrate how the OT error can quantify this trade-off for the bike sharing data. In bike sharing research, there is indeed a lack of comparability of previous work due to different aggregation schemes, ranging from single-station prediction [113, 78] to various clustering schemes [42, 93, 57]. To capture this variety, we also aggregate the bike sharing data with several methods, namely 1) grouping by sociological or housing district¹, 2) clustering with the KMeans algorithm (varying k), and 3) clustering with hierarchical (Agglomerative) clustering using different cutoffs. The bike sharing demand of a

¹sociological districts from <https://www.donneesquebec.ca/recherche/dataset/vmt1-quartiers-sociologiques> and housing districts according to <https://www.donneesquebec.ca/recherche/dataset/vmt1-quartiers>

cluster is the sum of the demand of all its associated stations. One model is trained per configuration, where again the N-HiTS time series prediction model is used. The results are evaluated on the same test time points as before.

As illustrated in Figure 8, we consider three evaluation methods: the MSE between cluster-level predictions, the OT cost from clusters to points, and the OT error on a point-level. The results for the first method, representing the standard approach taken in related work, are shown in Figure 8A. The MSE decreases as the number of clusters increases because each cluster contains fewer observations, which typically results in smaller errors per cluster. When normalizing the errors by the respective cluster size, the opposite effect can be observed: The larger the clusters, the smaller the normalized errors, since larger clusters exhibit more regular patterns and are easier to predict (see Appendix F). Thus, there is no MSE-based method that can quantify the trade-off between predictability and the utility.

To address this problem with OT, we first compute the OT error² for transporting from cluster-predictions to station observations (see Figure 8 blue). In the context of bike-sharing, this is analogous to situating distribution hubs at the center of each cluster. In this case, the OT error decreases with higher granularity (see Figure 8B), because all mass needs to be moved from the cluster centers to individual stations, whereas in station-wise prediction, some of the mass remains stationary. A bike sharing company could add this cost to the expenses of establishing distribution centers, balancing the operational costs of more centers against their reduced OT expense. Secondly, we compute the OT error after transforming cluster-wise predictions into forecasts at individual stations (see Figure 8 orange). Here, the value assigned to each station is determined based on their average demand in the training set relative to the demand of other stations within the same cluster. Figure 8C demonstrates that the OT error depends on the clustering technique and cluster size, with a minimum at 150 clusters created through Agglomerative clustering. This configuration seems to optimize prediction accuracy while maintaining desirable granularity. The OT-based evaluation framework thus improves comparability of prediction methods across scales, supporting users in selecting the most appropriate aggregation method for their use cases.

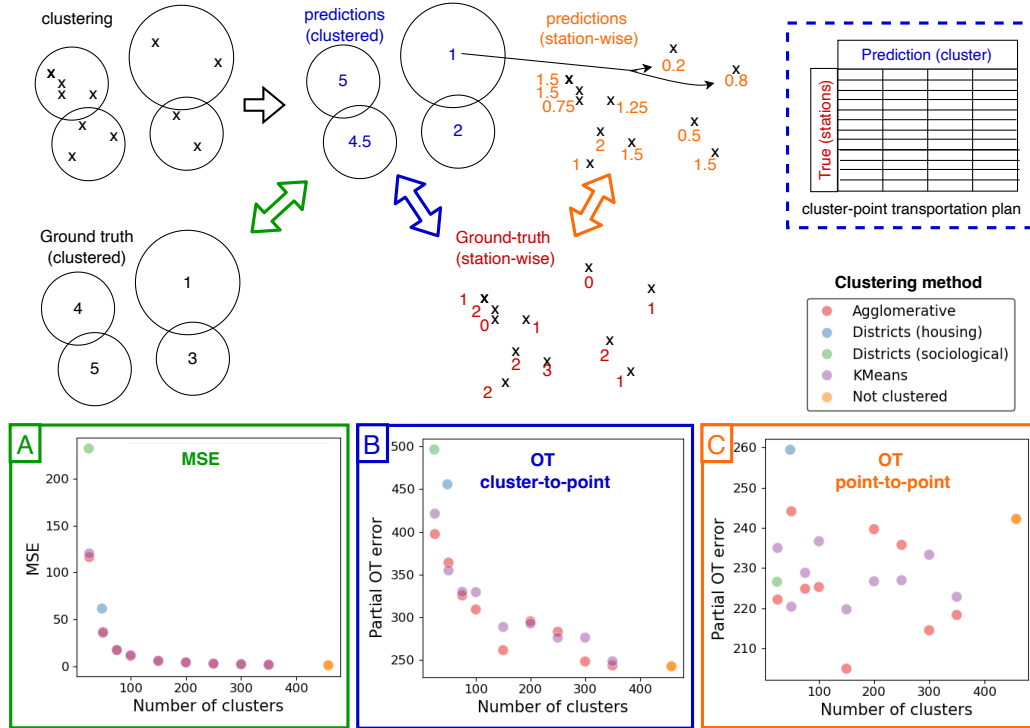


Figure 8: Comparing the prediction quality across spatial aggregation scales. The errors for bike sharing demand prediction are shown for varying station clusterings. The MSE is not comparable across aggregation schemes since higher granularity simply results in lower errors (A). Optimal transport allows for asymmetric cost matrices (blue) to compute the costs for transporting from prediction-clusters to the ground-truth-points (B). In addition, OT computed on the station-mapped predictions (orange) draws a more complex picture of the prediction quality for different aggregation schemes (C).

²Here, we use W_c^{geo} with ϕ equivalent to the 10%-quantile of C (see Appendix E) to model realistic business costs that arise mainly from redistribution but partly from a general over- or underestimation of bike sharing demand.

3.3.2 Comparability between space and time

Time and space are currently treated as independent dimensions when evaluating spatio-temporal prediction models. For example, when predicting bike sharing demand for the next five hours, the errors are usually reported as averages over time and over locations. To the best of our knowledge, there are no methods to compare inaccuracies in time (e.g., predicting high demand for a later time than when it actually emerges) to inaccuracies in space (e.g., overestimating the demand at station A while underestimating station B). We suggest to enable the joint evaluation of spatial and temporal errors with OT, by translating relocation costs into relocation *time*. The proposed costs are visually explained in Figure 9 and detailed in the following. We first define the cost matrix \mathbf{C} in terms of time instead of distance. For the bike sharing example, we derive the walking time from the spatial distances of locations by assuming a walking speed of 5km/h. We now extend the spatial cost matrix to a space-time cost matrix Ψ . Let $\Psi_{(i,t_k),(j,t_l)}$ be the time to relocate from the i -th location at time t_k to the j -th location at time t_l . Dependent to the specific application, it must be decided how to penalize *temporal* errors - what is the cost for $\Psi_{(i,t_k),(i,t_l)}$, i.e. the transport of mass from one time point to another? A simple option is to set the temporal relocation cost to $|t_k - t_l|$ (see Figure 9). This could be viewed as a *waiting* time until a bike becomes available. Finally, we suggest to combine both components by setting the time-space-relocation cost to the maximum of both parts, since bike sharing users can wait until a bike is available and relocate to another station during the same time period. The final cost matrix is thus defined as $\Psi_{(i,t_k),(j,t_l)} = \max\{C_{ij}, |t_k - t_l|\}$.

In Table 2, the N-HiTS model is compared to a linear regression model in their performance of forecasting the bike sharing demand for the next five hours. We evaluate 100 test samples, where each sample comprises all stations for these five time steps, in terms of the MSE (averaging across locations and time), the spatial W_c^{geo} (average over the five time steps), and the spatio-temporal W_c^{geo} . The results show that the spatial W_c^{geo} of the linear model is only 18% larger than the one for N-HiTS, whereas the spatio-temporal error increases by 30% (67.62 vs 52.14). This result indicates that the N-HiTS model indeed excels in accurate multi-step forecasting due to its hierarchical learning process. More general, this framework allows to quantify and compare temporal and spatial shifts of models proposed for spatio-temporal prediction tasks.

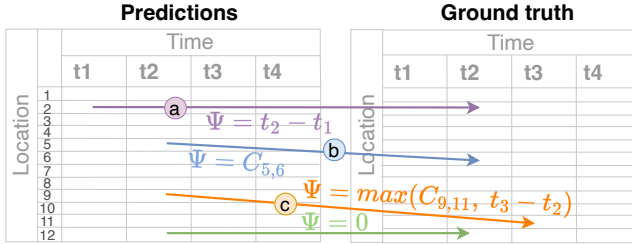


Figure 9: OT across space and time. Spatio-temporal cost (c) combines temporal cost (a, e.g. waiting time), with spatial cost (b, e.g. relocation time).

	N-HiTS	Linear regression
spatial W_c^{geo} (mean)	39.05	46.07
spatio-temporal W_c^{geo}	52.14	67.62
MSE	1.24	1.94

Table 2: Model comparison by spatial and spatio-temporal OT error. N-HiTS particularly improves the spatio-temporal error.

4 OT metrics as a loss function in GeoAI

A natural progression for the OT error is its integration into the *training* of neural networks as a spatial loss function. In the following, we explain the Sinkhorn divergence allowing to train with OT, and present experiments on three datasets.

4.1 Training with the Sinkhorn divergence

4.1.1 The Sinkhorn algorithm

As discussed in § 2.1, OT provides a discrepancy measure between two distribution μ, ν . On the other hand, although solvable as a linear program, Problem (1) presents some challenges. Firstly, the time complexity of the network simplex algorithm scales as $\mathcal{O}(nm(n+m)\log(n+m))$, where n is the support size of the source distribution μ and m is that of the target distribution ν . This complexity restricts its applicability to a large number of locations. Secondly, the solution \mathbf{T}^* to the OT problem 1 is not necessarily unique. Consequently, W_c is non-differentiable with respect to its inputs, i.e., non-differentiable with respect to the \mathbf{x}_i and \mathbf{y}_j locations of the μ and ν support, as well as the weight vectors \mathbf{p} and \mathbf{q} . As a result, these challenges limit the direct use of W_c as a loss function. One way to alleviate these challenges is to rely on entropic regularization [21]. Introducing $H(\mathbf{T}) = \sum_{i,j=1}^{n,m} \mathbf{T}_{ij} \log(\mathbf{T}_{ij})$ and $\varepsilon > 0$, we define the

Entropic OT problem between $\mu = \sum_{i=1}^n \mathbf{p}_i \delta_{\mathbf{x}_i}$ and $\nu = \sum_{i=1}^m \mathbf{q}_i \delta_{\mathbf{y}_i}$ as

$$W_{c,\varepsilon}(\mu, \nu) = \min_{\mathbf{T} \in \mathcal{U}(\mathbf{p}, \mathbf{q})} \langle \mathbf{T}, \mathbf{C} \rangle - \varepsilon H(\mathbf{T}). \quad (11)$$

Here, ε controls the regularization strength. For $\varepsilon \rightarrow 0$, one recovers the standard Wasserstein distance, namely $W_{c,\varepsilon}(\mu, \nu) \rightarrow W_c(\mu, \nu)$. The Entropic OT Prob. 11 admits a dual formulation, which takes the form of an unconstrained, ε -strongly concave program

$$W_{c,\varepsilon}(\mu, \nu) = \max_{\mathbf{f} \in \mathbb{R}^n, \mathbf{g} \in \mathbb{R}^m} \langle \mathbf{f}, \mathbf{p} \rangle + \langle \mathbf{g}, \mathbf{q} \rangle - \varepsilon \langle e^{\mathbf{f}/\varepsilon}, \mathbf{K} e^{\mathbf{g}/\varepsilon} \rangle, \quad (12)$$

where $\mathbf{K} = [\exp(-c(\mathbf{x}_i, \mathbf{y}_j)/\varepsilon)]_{1 \leq i, j \leq n, m} \in \mathbb{R}_+^{n \times m}$ and $e^{\mathbf{f}}, e^{\mathbf{g}}$ denotes the element-wise exponential of the vectors \mathbf{f}, \mathbf{g} . By strong concavity, the optimal $\mathbf{f}^*, \mathbf{g}^*$ exist and are unique.

[Sinkhorn](#)'s algorithm provides an iterative approach for finding $(\mathbf{f}^*, \mathbf{g}^*)$, which we summarize in Algorithm 1. For a matrix $\mathbf{A} = [\mathbf{A}_{ij}]_{1 \leq i, j \leq n, m}$, we define the (rowwise) ε -soft-min operator as: $\min_\varepsilon(\mathbf{A}) := [-\varepsilon \log(\mathbf{1}^\top e^{-\mathbf{A}_{i,\cdot}/\varepsilon})]_{1 \leq i \leq n}$, and \oplus denotes the tensor sum of two vectors, i.e., $\mathbf{f} \oplus \mathbf{g} := [\mathbf{f}_i + \mathbf{g}_j]_{1 \leq i, j \leq n, m}$. Solving the dual Entropic OT Prob. (11) also provides a valid coupling through the primal-dual relationship: $\mathbf{T}_\varepsilon^* = \exp((\mathbf{C} - \mathbf{f}^* \oplus \mathbf{g}^*)/\varepsilon)$. Since [Sinkhorn](#)'s algorithm essentially alternates between matrix-vector multiplications, its computational complexity scales as $\mathcal{O}(nm)$. Similarly, the memory complexity is also $\mathcal{O}(nm)$, as the cost matrix \mathbf{C} must be stored.

By [Danskin](#)'s Theorem, the uniqueness of \mathbf{f}^* and \mathbf{g}^* guarantees the differentiability of $W_{c,\varepsilon}(\mu, \nu)$ with respect to its inputs. Moreover, we treat \mathbf{f}^* and \mathbf{g}^* as constants during differentiation. As a result, there is no need to back-propagate through [Sinkhorn](#)'s algorithm. Formally, for any input \blacksquare , that can be a location $\mathbf{x}_i, \mathbf{y}_j$, or a weight vector \mathbf{p}, \mathbf{q} , one has:

$$\nabla_{\blacksquare} W_{c,\varepsilon}(\mu, \nu) = \nabla_{\blacksquare} \langle \mathbf{f}^*, \mathbf{p} \rangle + \nabla_{\blacksquare} \langle \mathbf{g}^*, \mathbf{q} \rangle - \varepsilon \nabla_{\blacksquare} \langle e^{\mathbf{f}^*/\varepsilon}, \mathbf{K} e^{\mathbf{g}^*/\varepsilon} \rangle, \quad (13)$$

where both \mathbf{f}^* and \mathbf{g}^* are treated as constants with respect to \blacksquare . For instance, the gradients with respect to the weight vectors \mathbf{p}, \mathbf{q} , which are used in our method, are given by:

$$\begin{aligned} \nabla_{\mathbf{p}} W_{c,\varepsilon}(\mu, \nu) &= \nabla_{\mathbf{p}} \langle \mathbf{f}^*, \mathbf{p} \rangle = \mathbf{f}^* \\ \nabla_{\mathbf{q}} W_{c,\varepsilon}(\mu, \nu) &= \nabla_{\mathbf{q}} \langle \mathbf{g}^*, \mathbf{q} \rangle = \mathbf{g}^* \end{aligned} \quad (14)$$

4.1.2 The Sinkhorn divergence

We recall that when $c(\mathbf{x}, \mathbf{y}) = \|\mathbf{x} - \mathbf{y}\|_2$ or $c(\mathbf{x}, \mathbf{y}) = \|\mathbf{x} - \mathbf{y}\|_2^2$, $W_c(\mu, \nu) \geq 0$ with equality if and only if $\mu = \nu$. This property is central to our approach, as it justifies the use of W_c for comparing distributions. However, this property does not hold when entropy regularization is introduced, as $W_{c,\varepsilon}(\mu, \nu)$ can become negative, and in general, $W_{c,\varepsilon}(\mu, \mu) \neq 0$. As a result, this introduces a bias that complicates the use of $W_{c,\varepsilon}$ as a loss function.

In light of this phenomenon, several works [[35](#), [29](#), [75](#)] have proposed centering the Entropic OT objective, thereby defining the Sinkhorn divergence as follows:

$$S_{c,\varepsilon}(\mu, \nu) = W_{c,\varepsilon}(\mu, \nu) - \frac{1}{2}(W_{c,\varepsilon}(\mu, \mu) + W_{c,\varepsilon}(\nu, \nu)) \quad (15)$$

Centering the Entropic OT objective is akin to debiasing it. For example, when $c(\mathbf{x}, \mathbf{y}) = \|\mathbf{x} - \mathbf{y}\|_2$ or $c(\mathbf{x}, \mathbf{y}) = \|\mathbf{x} - \mathbf{y}\|_2^2$, the following holds [[29](#), Theorem 1]

$$S_{c,\varepsilon}(\mu, \nu) \geq 0 \text{ with equality if and only if } \mu = \nu. \quad (16)$$

Additionally, the two corrective terms $-W_{c,\varepsilon}(\mu, \mu)$ and $-W_{c,\varepsilon}(\nu, \nu)$ can be computed even more efficiently than by directly using the Sinkhorn algorithm 1. As noted by Feydy et al. [[29](#)], the key observation is that when $\mu = \nu$, the dual Prob. (12) reduces to a concave maximization problem with respect to a single variable. This can be solved by iterating a well-conditioned fixed-point update, which typically converges to the desired precision within three iterations.

In practice, we use the default Sinkhorn divergence implementation provided in the `geomloss` package [[29](#)], which employs the Sinkhorn algorithm 1 and leverages the trick to efficiently compute the corrective terms. This loss function is plugged into the N-HiTS time series prediction model [[13](#)], leaving all other model settings unchanged (see [Appendix D](#)).

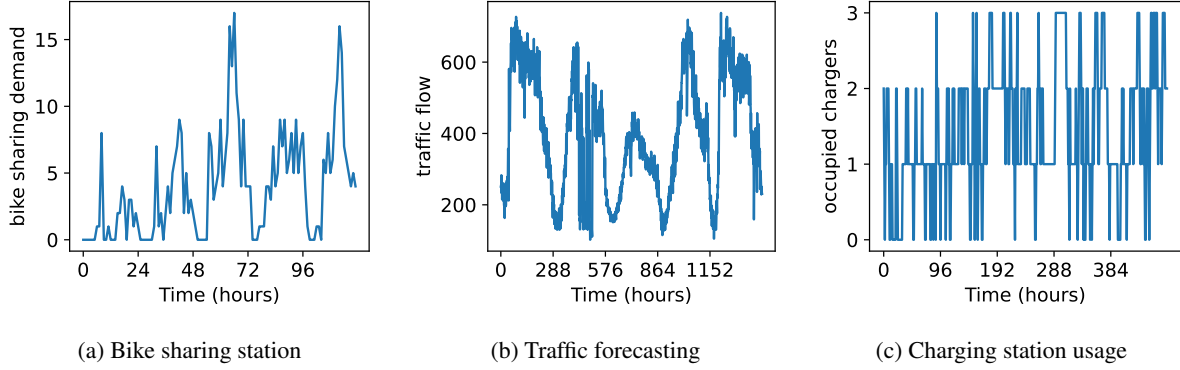


Figure 10: Example time series for the three tested applications. Each plot shows the time series at one location for an excerpt of five days. At the respective location, up to 17 bikes are picked up per hour (a), the traffic flow varies between 200 and 600 (b), and usually 1-2 plugs of the charging station are occupied (c).

4.2 Data and experimental setup

We train the N-HITS model with the Sinkhorn divergence and compare the results to the ones obtained previously when training with an MSE loss. For a more comprehensive picture, we consider three applications: bike sharing demand, charging station occupancy, and traffic flow forecasting. A dataset on EV charging stations was published by Amara-Ouali et al. [3]. It provides the charging station occupancy for 83 stations in France from July 2020 to February 2021 at a granularity of 15 minutes. For traffic forecasting, we use the popular PEMS dataset of traffic detectors on freeways in California. We take a small version of the dataset comprising 163 sensors and extract solely the traffic flow values that are available at a granularity of 5 min. Figure 10 shows a five-days excerpt of the respective time series for the three applications. The models were trained to predict the demand for the next five time steps. For details on the data sources, preprocessing and the model training, see Appendix C and Appendix D. While OT has been used for evaluating spatio-temporal forecasts [80], to the best of our knowledge, this is the first attempt to improve forecasts of geospatial data with a Sinkhorn divergence function.

4.3 Results

Table 3 presents the results on test data in terms of the MSE, the balanced OT cost (scaling Y and \hat{Y} to have equal sums), and W_c^{geo} with small and large ϕ (see Appendix E for further analysis on the choice of ϕ and its effect on W_c^{geo}). The cost matrix C was set to the Euclidean distance between stations in km. This results in an interpretable model performance. For example, a relocation effort of around 135.7km is required in total to align the predicted bike sharing demand with the true one. As desired, training with an OT-based loss function decreases the OT costs, with a minor effect on the MSE. For the charging station application, the MSE succeeds over a Sinkhorn divergence in minimizing the total error δ ; thus, only W_c^{geo} decreases with a Sinkhorn divergence. For bike sharing demand prediction and traffic forecasting, all OT-based metrics are improved significantly when training with a Sinkhorn divergence.

Application	Loss function	MSE	W_c^{geo}	$W_{\phi,c}^{geo} (\phi \text{ low})$	$W_{c,\phi}^{geo} (\phi \text{ high})$
Bike sharing demand	OT (Sinkhorn) loss	1.26	135.7	195.7	1733.8
	MSE loss	1.24	161.5	242.2	2406.1
Charging station occupancy	OT (Sinkhorn) loss	0.35	30.7	30.8	87.0
	MSE loss	0.34	32.7	30.7	81.1
Traffic flow	OT (Sinkhorn) loss	876.63	1629.3	1565.9	5558.4
	MSE loss	852.53	1639.3	1598.2	5892.3

Table 3: Results when training with an OT-based loss function. At minor increase of the MSE, OT-based metrics can be decreased substantially; e.g., from 161.5 to 135.7km bike relocation cost.

Figure 11 provides an example for the resulting transportation matrices for one time point of the traffic prediction task. For visualization purposes, only a subset of the the traffic sensors is shown, selected by spectral clustering on the

distance matrix and randomly choosing one cluster. The comparison of the transportation costs in both cases shows that the Sinkhorn divergence model improves over the MSE-loss model, resulting in lower transportation costs in this example (see Figure 11 right).

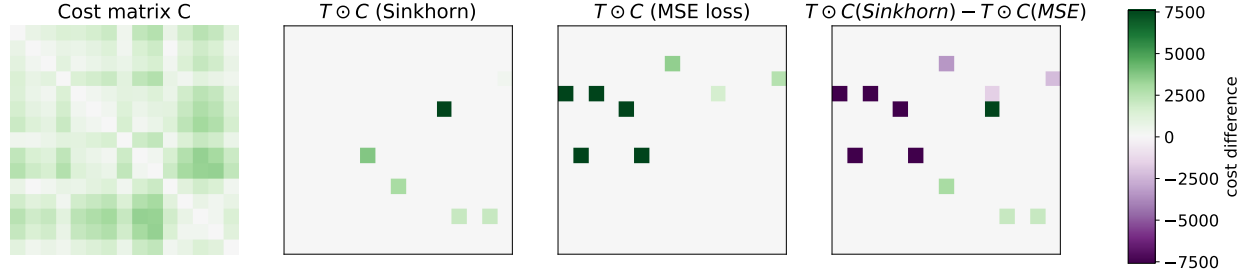


Figure 11: Transportation costs for aligning traffic flow predictions with the ground truths. The plot compares the results between a model trained with an MSE loss to a model trained with the Sinkhorn divergence. \odot denotes the element-wise multiplication of two matrices; here the OT matrix T and the cost matrix C .

5 Discussion

Optimal Transport holds significant potential to incorporate spatial considerations into both the evaluation and training of GeoAI models. First, OT provides *interpretable* error metrics linked to operational costs, making it valuable for practical applications. Second, OT inherently accounts for *spatial* relationships, serving as a spatially-explicit metric that evaluates prediction errors in the context of their locality. Last, its *flexibility* allows for customization to specific applications through the use of tailored cost functions.

The decision how to implement OT metrics should consider the specific prediction problem and the use of predictions in downstream tasks. Its relevance varies across applications; for instance, it is particularly useful for evaluating predictions of transport demand, but less so in traffic forecasting, where the spatial distribution of errors is less critical. To determine its applicability, we recommend to construct a cost matrix with a certain real-world meaning (e.g., relocations, mission planning, signal control, interventions). If there exists such cost matrix with obvious real-world relevance, an OT-based evaluation is clearly suitable. At the same time, OT metrics are even useful without any real-world interpretation due to their ability to reflect spatial autocorrelation. This allows to evaluate models by their ability to deal with spatial heterogeneity of the data.

While OT is generally applicable to spatio-temporal prediction problems, there are some limitations and challenges. First, OT cannot deal with negative values; however, this problem can usually be resolved with a simple scaling of all values. Secondly, a pivotal choice in our framework concerns the value of ϕ , i.e. the costs for importing or exporting mass in partial OT. A smaller ϕ emphasizes accuracy in spatial distribution over the minimization of total error. Selectively adjusting ϕ by application poses a risk for cherry-picking; i.e. setting ϕ to the value with the best results. While further analysis is required to gain a better understanding of the dependency of the error on ϕ , our preliminary tests in Appendix E suggest to set ϕ to the maximum value of the cost matrix.

Finally, our investigation predominantly explores regression scenarios, highlighting the potential of OT in forecasting the distribution or “mass” at given coordinates and times. Its utility extends to classification tasks, as shown in an application on deforestation prediction in Appendix B; however, further work is necessary to assess the applicability of OT for other GeoAI problems. In particular, calculating the OT error is computationally more expensive than other metrics. While modern LP solvers and the Sinkhorn algorithm generally offset these concerns, challenges may arise when handling datasets with numerous locations, such as high-resolution remote sensing imagery. While evaluation metrics are usually not required to be particularly fast, implementing OT-based loss functions could notably decelerate neural network training. Our work provides guidelines on possible research avenues and outlines general advantages over non-spatial metrics, but further research is required to substantiate these advantages in specific real-world applications.

6 Conclusion

In compliance with Tobler’s law that near things are more related than distant things [100], this paper introduces a spatial metric for evaluating spatio-temporal predictions. It leverages Optimal Transport theory, an established mathematical field with a strong theoretical foundation. Our experiments on synthetic and real data demonstrated the value of OT for

geospatial contexts, showcasing its real-world meaning due to its quantification of the potential cost reductions, its ability to incorporate application-specific criteria with arbitrary cost matrices, its relation to key geographical concepts such as spatial autocorrelation, and its utility as a loss function.

There are numerous paths for future work. A first step to establish OT as an evaluation metric in specific GIS fields involves reviewing existing methodologies and comparing them with respect to OT costs. Additionally, we have showcased and briefly demonstrated several promising directions, such as integrating space and time into a unified OT cost metric, which should be investigated in more detail. Moreover, the combination of OT and GIS is not a one-way street, since some of the presented ideas are interesting for a more general machine learning audience. For example, the proposed concept of space-time-cost matrices implies that there is a use case in general time series analysis beyond spatial data. In any multi-step time series prediction task, OT could be used to quantify the temporal prediction inaccuracies. A second example is the uncovered connection between OT and Moran’s I, which not only supports the utility of OT in GIS, but also indicates the potential of Moran’s I for approximating the OT error in non-spatial (and potentially high-dimensional data) scenarios. Last, our experiments with the Sinkhorn divergence show the potential of a wider application of OT-based loss functions with location-based cost matrices, such as in remote sensing.

Ultimately, we not only aim to convince GIS practitioners and GeoAI researchers of the value of the OT-based evaluation framework, but stimulate further research into its application-specific uses, domain-independent applications, and into enhancing model training with OT-based approaches.

Acknowledgements

We would like to thank Thomas Spanniger for the fruitful discussions and valuable feedback. This project is part of the E-Bike City project funded by the Department of Civil and Environmental Engineering (D-BAUG) at ETH Zurich and the Swiss Federal Office of Energy (BFE).

Data and code availability

All code is publicly available at https://github.com/mie-lab/geospatial_optimal_transport/ and, as a tutorial version, at <https://github.com/mie-lab/geospatialOT>. All datasets are publicly available as detailed in [Appendix C](#).

References

- [1] M. Abouelela, C. Lyu, and C. Antoniou. Exploring the potentials of open-source big data and machine learning in shared mobility fleet utilization prediction. *Data Science for Transportation*, 5(2):5, 2023.
- [2] A. Alem and S. Kumar. Deep learning methods for land cover and land use classification in remote sensing: A review. In *2020 8th International Conference on Reliability, Infocom Technologies and Optimization (Trends and Future Directions) (ICRITO)*, pages 903–908. IEEE, 2020.
- [3] Y. Amara-Ouali, Y. Goude, N. Doumèche, P. Veyret, A. Thomas, D. Hebenstreit, T. Wedenig, A. Satouf, A. Jan, Y. Deleuze, et al. Forecasting electric vehicle charging station occupancy: Smarter mobility data challenge. *arXiv preprint arXiv:2306.06142*, 2023.
- [4] G. Athanasopoulos and N. Kourentzes. On the evaluation of hierarchical forecasts. *International Journal of Forecasting*, 39(4):1502–1511, 2023.
- [5] D. Bertsimas and J. Tsitsiklis. *Introduction to linear optimization*. Athena Scientific, 1997.
- [6] V. D. Bortoli, G.-H. Liu, T. Chen, E. A. Theodorou, and W. Nie. Augmented bridge matching. *arXiv preprint arXiv:2311.06978*, 2023.
- [7] N. Brahim, H. Zhang, L. Dai, and J. Zhang. Modelling on car-sharing serial prediction based on machine learning and deep learning. *Complexity*, 2022(1):8843000, 2022.
- [8] C. Bunne, S. G. Stark, G. Gut, J. S. del Castillo, K.-V. Lehmann, L. Pelkmans, A. Krause, and G. Ratsch. Learning single-cell perturbation responses using neural optimal transport. *bioRxiv*, 2021.
- [9] C. Bunne, L. Papaxanthos, A. Krause, and M. Cuturi. Proximal Optimal Transport modeling of population dynamics. In *International Conference on Artificial Intelligence and Statistics*, pages 6511–6528. PMLR, 2022.
- [10] C. Bunne, S. G. Stark, G. Gut, J. S. Del Castillo, M. Levesque, K.-V. Lehmann, L. Pelkmans, A. Krause, and G. Ratsch. Learning single-cell perturbation responses using neural optimal transport. *Nature Methods*, 20(11):1759–1768, 2023.

- [11] M. Buzzelli. Modifiable Areal Unit Problem. *International encyclopedia of human geography*, page 169, 2020.
- [12] K. Cao, Q. Gong, Y. Hong, and L. Wan. A unified computational framework for single-cell data integration with optimal transport. *Nature Communications*, 13(1):7419, 2022.
- [13] C. Challu, K. G. Olivares, B. N. Oreshkin, F. Garza, M. Mergenthaler-Canseco, and A. Dubrawski. N-HiTS: Neural hierarchical interpolation for time series forecasting. *arXiv preprint arXiv:2201.12886*, 2022.
- [14] L. Chapel, M. Z. Alaya, and G. Gasso. Partial optimal transport with applications on positive-unlabeled learning. *Advances in Neural Information Processing Systems*, 33:2903–2913, 2020.
- [15] L. Chapel, R. Flamary, H. Wu, C. Févotte, and G. Gasso. Unbalanced Optimal Transport through non-negative penalized linear regression. *Advances in Neural Information Processing Systems*, 34:23270–23282, 2021.
- [16] Y. Chen. Spatial autocorrelation approaches to testing residuals from least squares regression. *PloS one*, 11(1): e0146865, 2016.
- [17] A. Chin and Z. Qin. A unified representation framework for rideshare marketplace equilibrium and efficiency. *arXiv preprint arXiv:2302.14358*, 2023.
- [18] L. Chizat, G. Peyré, B. Schmitzer, and F. Vialard. Scaling algorithms for unbalanced Optimal Transport problems. *Mathematics of Computation*, 87(314):2563–2609, 2018.
- [19] Y.-H. Chou. Critical issues in the evaluation of spatial autocorrelation. In *European Conference on Spatial Information Theory*, pages 421–433. Springer, 1993.
- [20] A. Cuttone, S. Lehmann, and M. C. González. Understanding predictability and exploration in human mobility. *EPJ Data Science*, 7(1):2, 2018.
- [21] M. Cuturi. Sinkhorn distances: Lightspeed computation of Optimal Transport. In *Advances in Neural Information Processing Systems*, volume 26. Curran Associates, Inc., 2013.
- [22] Z. Dang, F. Wang, and M. Salzmann. Learning 3d-3d correspondences for one-shot partial-to-partial registration. *arXiv preprint arXiv:2006.04523*, 2020.
- [23] J. M. Danskin. *The Theory of Max-Min and its Applications to Weapons Allocation Problems*, volume 5. Springer, 1967.
- [24] V. De Bortoli, J. Thornton, J. Heng, and A. Doucet. Diffusion schrödinger bridge with applications to score-based generative modeling. *Advances in Neural Information Processing Systems*, 34:17695–17709, 2021.
- [25] H. De Plaen, P.-F. De Plaen, J. A. K. Suykens, M. Proesmans, T. Tuytelaars, and L. Van Gool. Unbalanced Optimal Transport: A unified framework for object detection. In *Proceedings of the IEEE/CVF Conference on Computer Vision and Pattern Recognition (CVPR)*, pages 3198–3207, June 2023.
- [26] P. Demetci, R. Santorella, B. Sandstede, W. S. Noble, and R. Singh. SCOT: single-cell multi-omics alignment with Optimal Transport. *Journal of Computational Biology*, 29(1):3–18, 2022.
- [27] L. Eyring, D. Klein, T. Uscidda, G. Palla, N. Kilbertus, Z. Akata, and F. Theis. Unbalancedness in neural monge maps improves unpaired domain translation. *arXiv preprint arXiv:2311.15100*, 2024.
- [28] S. Fathimabi, G. JayaLakshmi, M. Suneetha, et al. Spatial data mining for prediction of unobserved zinc pollutants using various kriging methods. *Journal of Advanced Environmental Research and Technology*, 1(3): 57–67, 2023.
- [29] J. Feydy, T. Séjourné, F.-X. Vialard, S.-i. Amari, A. Trouvé, and G. Peyré. Interpolating between Optimal Transport and MMD using Sinkhorn divergences. In *The 22nd International Conference on Artificial Intelligence and Statistics*, pages 2681–2690. PMLR, 2019.
- [30] A. S. Fotheringham and D. W. S. Wong. The Modifiable Areal Unit Problem in multivariate statistical analysis. *Environment and Planning A: Economy and Space*, 23(7):1025–1044, 1991.
- [31] A. Galichon. *Optimal Transport Methods in Economics*. Princeton University Press, 2016.
- [32] F. Gao, S. Li, Z. Tan, Z. Wu, X. Zhang, G. Huang, and Z. Huang. Understanding the Modifiable Areal Unit Problem in dockless bike sharing usage and exploring the interactive effects of built environment factors. *International Journal of Geographical Information Science*, 35(9):1905–1925, 2021.
- [33] Z. Ge, S. Liu, Z. Li, O. Yoshie, and J. Sun. OTA: Optimal Transport assignment for object detection. *arXiv preprint arXiv:2103.14259*, 2021.
- [34] C. E. Gehlke and K. Biehl. Certain effects of grouping upon the size of the correlation coefficient in census tract material. *Journal of the American Statistical Association*, 29(185A):169–170, 1934.

- [35] A. Genevay, G. Peyré, and M. Cuturi. Learning generative models with sinkhorn divergences. In *International Conference on Artificial Intelligence and Statistics*, pages 1608–1617. PMLR, 2018.
- [36] K. Guittet. Extended Kantorovich norms: a tool for optimization. *Dissertation, INRIA*, 2002.
- [37] S. Guo, Y. Lin, H. Wan, X. Li, and G. Cong. Learning dynamics and heterogeneity of spatial-temporal graph data for traffic forecasting. *IEEE Transactions on Knowledge and Data Engineering*, 34(11):5415–5428, 2021.
- [38] M. Heitz, N. Bonneel, D. Coeurjolly, M. Cuturi, and G. Peyré. Ground metric learning on graphs. *Journal of Mathematical Imaging and Vision*, pages 1–19, 2020.
- [39] J. Herzen, F. Lässig, S. G. Piazzetta, T. Neuer, L. Tafti, G. Raille, T. Van Pottelbergh, M. Pasieka, A. Skrodzki, N. Huguenin, et al. Darts: User-friendly modern machine learning for time series. *The Journal of Machine Learning Research*, 23(1):5442–5447, 2022.
- [40] Y. Hu, S. Gao, D. Lunga, W. Li, S. Newsam, and B. Bhaduri. GeoAI at ACM SIGSPATIAL: progress, challenges, and future directions. *Sigspatial Special*, 11(2):5–15, 2019.
- [41] C.-W. Huang, R. T. Q. Chen, C. Tsirigotis, and A. Courville. Convex potential flows: Universal probability distributions with optimal transport and convex optimization. In *International Conference on Learning Representations (ICLR)*, 2021.
- [42] P. Hulot, D. Aloise, and S. D. Jena. Towards station-level demand prediction for effective rebalancing in bike-sharing systems. In *Proceedings of the 24th ACM SIGKDD international conference on knowledge discovery & data mining*, pages 378–386, 2018.
- [43] R. J. Hyndman, R. A. Ahmed, G. Athanasopoulos, and H. L. Shang. Optimal combination forecasts for hierarchical time series. *Computational Statistics & Data Analysis*, 55(9):2579–2589, 2011.
- [44] H. Janati, T. Bazeille, B. Thirion, M. Cuturi, and A. Gramfort. Multi-subject meg/eeeg source imaging with sparse multi-task regression. *NeuroImage*, 220:116847, 2020.
- [45] H. Janati, M. Cuturi, and A. Gramfort. Spatio-temporal alignments: Optimal Transport through space and time. In *International Conference on Artificial Intelligence and Statistics*, pages 1695–1704. PMLR, 2020.
- [46] K. Janowicz, S. Gao, G. McKenzie, Y. Hu, and B. Bhaduri. GeoAI: spatially explicit artificial intelligence techniques for geographic knowledge discovery and beyond. *International Journal of Geographical Information Science*, 34(4):625–636, 2020.
- [47] L. V. Kantorovich and S. Rubinshtein. On a space of totally additive functions. *Vestnik of the St. Petersburg University: Mathematics*, 13(7):52–59, 1958.
- [48] S. Kareem, Z. J. Hamad, and S. Askar. An evaluation of CNN and ANN in prediction weather forecasting: A review. *Sustainable Engineering and Innovation*, 3(2):148–159, 2021.
- [49] P. Kassraie, A.-A. Pooladian, M. Klein, J. Thornton, J. Niles-Weed, and M. Cuturi. Progressive entropic optimal transport solvers, 2024.
- [50] G. Ke, Q. Meng, T. Finley, T. Wang, W. Chen, W. Ma, Q. Ye, and T.-Y. Liu. Lightgbm: A highly efficient gradient boosting decision tree. *Advances in neural information processing systems*, 30, 2017.
- [51] M. Khalesian, A. Furno, and L. Leclercq. Improving deep-learning methods for area-based traffic demand prediction via hierarchical reconciliation. *Transportation Research Part C: Emerging Technologies*, 159:104410, 2024.
- [52] D. Klein, G. Palla, M. Lange, M. Klein, Z. Piran, M. Gander, L. Meng-Papaxanthos, M. Sterr, A. Bastidas-Ponce, M. Tarquis-Medina, et al. Mapping cells through time and space with moscot. *bioRxiv*, pages 2023–05, 2023.
- [53] D. Klein, T. Uscidda, F. Theis, and M. Cuturi. Entropic (Gromov) Wasserstein flow matching with GENOT. *arXiv preprint arXiv:2310.09254*, 2024.
- [54] A. Korotin, L. Li, J. Solomon, and E. Burnaev. Continuous Wasserstein-2 barycenter estimation without minimax optimization. *arXiv preprint arXiv:2102.01752*, 2021.
- [55] S. Koundal, R. Elkin, S. Nadeem, Y. Xue, S. Constantinou, S. Sanggaard, X. Liu, B. Monte, F. Xu, W. Van Nostrand, et al. Optimal mass transport with lagrangian workflow reveals advective and diffusion driven solute transport in the lymphatic system. *Scientific reports*, 10(1):1–18, 2020.
- [56] N. Kourentzes and G. Athanasopoulos. Cross-temporal coherent forecasts for Australian tourism. *Annals of Tourism Research*, 75:393–409, 2019.
- [57] Y. Li and Y. Zheng. Citywide bike usage prediction in a bike-sharing system. *IEEE Transactions on Knowledge and Data Engineering*, 32(6):1079–1091, 2020.

- [58] M. Liero, A. Mielke, and G. Savaré. Optimal entropy-transport problems and a new Hellinger–Kantorovich distance between positive measures. *Inventiones mathematicae*, 211(3):969–1117, 2018.
- [59] Y. Lipman, R. T. Q. Chen, H. Ben-Hamu, M. Nickel, and M. Le. Flow matching for generative modeling. *arXiv preprint arXiv:2210.02747*, 2023.
- [60] G.-H. Liu, A. Vahdat, D.-A. Huang, E. A. Theodorou, W. Nie, and A. Anandkumar. I²sb: Image-to-image schrödinger bridge. *arXiv preprint arXiv:2302.05872*, 2023.
- [61] G.-H. Liu, Y. Lipman, M. Nickel, B. Karrer, E. A. Theodorou, and R. T. Q. Chen. Generalized schrödinger bridge matching. *arXiv preprint arXiv:2310.02233*, 2024.
- [62] J. Liu, Q. Li, M. Qu, W. Chen, J. Yang, H. Xiong, H. Zhong, and Y. Fu. Station site optimization in bike sharing systems. In *2015 IEEE International Conference on Data Mining*, pages 883–888. IEEE, 2015.
- [63] P. Liu and F. Biljecki. A review of spatially-explicit GeoAI applications in urban geography. *International Journal of Applied Earth Observation and Geoinformation*, 112:102936, 2022.
- [64] Z. Liu, Q. Qiu, J. Li, L. Wang, and A. Plaza. Geographic Optimal Transport for heterogeneous data: Fusing remote sensing and social media. *IEEE Transactions on Geoscience and Remote Sensing*, 59(8):6935–6945, 2020.
- [65] T.-Y. Ma and S. Faye. Multistep electric vehicle charging station occupancy prediction using hybrid LSTM neural networks. *Energy*, 244:123217, 2022.
- [66] J. Maas, M. Rumpf, C. Schönlieb, and S. Simon. A generalized model for Optimal Transport of images including dissipation and density modulation. *ESAIM: Mathematical Modelling and Numerical Analysis*, 49(6):1745–1769, 2015.
- [67] A. Makkuva, A. Taghvaei, S. Oh, and J. Lee. Optimal transport mapping via input convex neural networks. In *International Conference on Machine Learning (ICML)*, volume 37, 2020.
- [68] P. A. Moran. Notes on continuous stochastic phenomena. *Biometrika*, 37(1/2):17–23, 1950.
- [69] N. Nakagawa, R. Togo, T. Ogawa, and M. Haseyama. Gromov-wasserstein autoencoders. *arXiv preprint arXiv:2209.07007*, 2023.
- [70] I. Peled, K. Lee, Y. Jiang, J. Dauwels, and F. C. Pereira. On the quality requirements of demand prediction for dynamic public transport. *Communications in Transportation Research*, 1:100008, 2021.
- [71] F. Petropoulos, D. Apiletti, V. Assimakopoulos, M. Z. Babai, and D. K. e. a. Barrow. Forecasting: theory and practice. *International Journal of Forecasting*, 38(3):705–871, 2022.
- [72] G. Peyré, M. Cuturi, et al. Computational Optimal Transport: With applications to data science. *Foundations and Trends® in Machine Learning*, 11(5-6):355–607, 2019.
- [73] K. Pham, K. Le, N. Ho, T. Pham, and H. Bui. On unbalanced Optimal Transport: An analysis of Sinkhorn algorithm. In *International Conference on Machine Learning*, pages 7673–7682. PMLR, 2020.
- [74] B. Piccoli and F. Rossi. Generalized Wasserstein distance and its application to transport equations with source. *Archive for Rational Mechanics and Analysis*, 211:335–358, 2014.
- [75] A.-A. Pooladian, M. Cuturi, and J. Niles-Weed. Debiaser beware: Pitfalls of centering regularized transport maps, 2022.
- [76] A.-A. Pooladian, H. Ben-Hamu, C. Domingo-Enrich, B. Amos, Y. Lipman, and R. Chen. Multisample flow matching: Straightening flows with minibatch couplings. *arXiv preprint arXiv:2304.14772*, 2023.
- [77] X. Qian, M. Jaller, and G. Circella. Exploring the potential role of bikeshare to complement public transit: The case of San Francisco amid the Coronavirus crisis. *Cities*, 137:104290, 2023.
- [78] S. Qiao, N. Han, J. Huang, K. Yue, R. Mao, H. Shu, Q. He, and X. Wu. A dynamic convolutional neural network based shared-bike demand forecasting model. *ACM Transactions on Intelligent Systems and Technology*, 12(6):1–24, 2021.
- [79] D. Radke, A. Hessler, and D. Ellsworth. Firecast: Leveraging deep learning to predict wildfire spread. In *IJCAI*, pages 4575–4581, 2019.
- [80] L. Roberts, L. Razoumov, L. Su, and Y. Wang. Gini-regularized Optimal Transport with an application to spatio-temporal forecasting. *arXiv preprint arXiv:1712.02512*, 2017.
- [81] Y. Rubner, C. Tomasi, and L. J. Guibas. The Earth Mover’s Distance as a metric for image retrieval. *Int. J. Comput. Vision*, 40(2):99–121, nov 2000.

- [82] M. Salis, B. Arca, F. Alcasena, M. Arianoutsou, V. Bacciu, P. Duce, B. Duguy, N. Koutsias, G. Mallinis, I. Mitsopoulos, et al. Predicting wildfire spread and behaviour in mediterranean landscapes. *International Journal of Wildland Fire*, 25(10):1015–1032, 2016.
- [83] M. E. Sander, P. Ablin, M. Blondel, and G. Peyré. Sinkformers: Transformers with doubly stochastic attention. *arXiv preprint arXiv:2110.11773*, 2022.
- [84] F. Santambrogio. Optimal transport for applied mathematicians. *Birkhäuser, NY*, 55(58-63):94, 2015.
- [85] F. Santos, V. Graw, and S. Bonilla. A geographically weighted random forest approach for evaluate forest change drivers in the northern ecuadorian amazon. *PLoS One*, 14(12):e0226224, 2019.
- [86] P.-E. Sarlin, D. DeTone, T. Malisiewicz, and A. Rabinovich. Superglue: Learning feature matching with graph neural networks. In *Proceedings of the IEEE/CVF conference on computer vision and pattern recognition*, pages 4938–4947, 2020.
- [87] G. Schiebinger, J. Shu, M. Tabaka, B. Cleary, V. Subramanian, A. Solomon, J. Gould, S. Liu, S. Lin, P. Berube, et al. Optimal-transport analysis of single-cell gene expression identifies developmental trajectories in reprogramming. *Cell*, 176(4), 2019.
- [88] G. Schiebinger, J. Shu, M. Tabaka, B. Cleary, V. Subramanian, A. Solomon, J. Gould, S. Liu, S. Lin, P. Berube, et al. Optimal-transport analysis of single-cell gene expression identifies developmental trajectories in reprogramming. *Cell*, 176(4), 2019.
- [89] M. A. Schmitz, M. Heitz, N. Bonneel, F. Ngole, D. Coeurjolly, M. Cuturi, G. Peyré, and J.-L. Starck. Wasserstein dictionary learning: Optimal Transport-based unsupervised nonlinear dictionary learning. *SIAM Journal on Imaging Sciences*, 11(1):643–678, 2018.
- [90] T. Séjourné, J. Feydy, F.-X. Vialard, A. Trounev, and G. Peyré. Sinkhorn divergences for unbalanced Optimal Transport. *arXiv preprint arXiv:1910.12958*, 2019.
- [91] Y. Shi, V. De Bortoli, A. Campbell, and A. Doucet. Diffusion schrödinger bridge matching. *arXiv preprint arXiv:2303.16852*, 2023.
- [92] D.-H. Shin, K. Chung, and R. C. Park. Prediction of traffic congestion based on LSTM through correction of missing temporal and spatial data. *IEEE Access*, 8:150784–150796, 2020.
- [93] B. Shir, J. Prakash Verma, and P. Bhattacharya. Mobility prediction for uneven distribution of bikes in bike sharing systems. *Concurrency and Computation: Practice and Experience*, 35(2):e7465, 2023.
- [94] R. Sinkhorn. A relationship between arbitrary positive matrices and doubly stochastic matrices. *Annals of Mathematical Statistics*, 35:876–879, 1964.
- [95] G. Smith, R. Wieser, J. Goulding, and D. Barrack. A refined limit on the predictability of human mobility. In *2014 IEEE International Conference on Pervasive Computing and Communications (PerCom)*, pages 88–94, 2014.
- [96] K. Smolak, K. Siła-Nowicka, J.-C. Delvenne, M. Wierzbinski, and W. Rohm. The impact of human mobility data scales and processing on movement predictability. *Scientific Reports*, 11(1):15177, 2021.
- [97] C. Sun and J. Lu. The relative roles of different land-use types in bike-sharing demand: A machine learning-based multiple interpolation fusion method. *Information Fusion*, 95:384–400, 2023.
- [98] Y. Tay, D. Bahri, L. Yang, D. Metzler, and D.-C. Juan. Sparse sinkhorn attention. *arXiv preprint arXiv:2002.11296*, 2020.
- [99] A. Thual, H. Tran, T. Zemskova, N. Courty, R. Flamary, S. Dehaene, and B. Thirion. Aligning individual brains with fused unbalanced gromov-wasserstein. *arXiv preprint arXiv:2206.09398*, 2023.
- [100] W. R. Tobler. A computer movie simulating urban growth in the detroit region. *Economic geography*, 46(sup1): 234–240, 1970.
- [101] A. Tong, J. Huang, G. Wolf, D. Van Dijk, and S. Krishnaswamy. TrajectoryNet: A dynamic optimal transport network for modeling cellular dynamics. In *International Conference on Machine Learning (ICML)*, 2020.
- [102] A. Tong, N. Malkin, K. Fatras, L. Atanackovic, Y. Zhang, G. Hugué, G. Wolf, and Y. Bengio. Simulation-free schrödinger bridges via score and flow matching. *arXiv preprint arXiv:2307.03672*, 2023.
- [103] A. Tong, N. Malkin, G. Hugué, Y. Zhang, J. Rector-Brooks, K. Fatras, G. Wolf, and Y. Bengio. Conditional flow matching: Simulation-free dynamic optimal transport. *arXiv preprint arXiv:2302.00482*, 2023.
- [104] K. Treleaven and E. Frazzoli. Computing Earth mover’s distances on a road map with applications to one-way vehicle sharing. In *2014 American Control Conference*, pages 5420–5427, 2014.

- [105] K. Treleaven, M. Pavone, and E. Frazzoli. Asymptotically optimal algorithms for one-to-one pickup and delivery problems with applications to transportation systems. *IEEE Transactions on Automatic Control*, 58(9): 2261–2276, 2013.
- [106] T. Uscidda and M. Cuturi. The Monge Gap: A regularizer to learn all transport maps. *arXiv preprint arXiv:2302.04953*, 2023.
- [107] T. Uscidda, L. Eyring, K. Roth, F. Theis, Z. Akata, and M. Cuturi. Disentangled representation learning through geometry preservation with the gromov-monge gap. *arXiv preprint arXiv:2407.07829*, 2024.
- [108] S. L. Wickramasuriya, G. Athanasopoulos, and R. J. Hyndman. Optimal Forecast Reconciliation for Hierarchical and Grouped Time Series Through Trace Minimization. *Journal of the American Statistical Association*, 114(526):804–819, 2019.
- [109] Y. Xiao, F. Ahmed, and Z. Sha. Graph neural network-based design decision support for shared mobility systems. *Journal of Mechanical Design*, pages 1–17, 2023.
- [110] P. Xu, H. Huang, and N. Dong. The Modifiable Areal Unit Problem in traffic safety: Basic issue, potential solutions and future research. *Journal of Traffic and Transportation Engineering (English Edition)*, 5(1):73–82, 2018.
- [111] R. Yan and S. Wang. Integrating prediction with optimization: Models and applications in transportation management. *Multimodal Transportation*, 1(3):100018, 2022.
- [112] K. D. Yang, K. Damodaran, S. Venkatachalapathy, A. C. Soylemezoglu, G. Shivashankar, and C. Uhler. Predicting cell lineages using autoencoders and optimal transport. *PLoS Computational Biology*, 16(4), 2020.
- [113] Z. Yang, J. Hu, Y. Shu, P. Cheng, J. Chen, and T. Moscibroda. Mobility modeling and prediction in bike-sharing systems. In *Proceedings of the 14th Annual International Conference on Mobile Systems, Applications, and Services*, pages 165–178, Singapore Singapore, 2016. ACM. ISBN 978-1-4503-4269-8.
- [114] W. Zeng, C. Lin, J. Lin, J. Jiang, J. Xia, C. Turkay, and W. Chen. Revisiting the Modifiable Areal Unit Problem in deep traffic prediction with visual analytics. *IEEE Transactions on Visualization and Computer Graphics*, 27(2):839–848, 2021.
- [115] L. Zhang, Z. Ma, and L. Guo. An evaluation of spatial autocorrelation and heterogeneity in the residuals of six regression models. *Forest Science*, 55(6):533–548, 2009.
- [116] F. Zhou, S. Luo, X. Qie, J. Ye, and H. Zhu. Graph-based equilibrium metrics for dynamic supply–demand systems with applications to ride-sourcing platforms. *Journal of the American Statistical Association*, 116(536): 1688–1699, 2021.
- [117] H. Zhu, Y. Luo, Q. Liu, H. Fan, T. Song, C. W. Yu, and B. Du. Multistep flow prediction on car-sharing systems: A multi-graph convolutional neural network with attention mechanism. *International Journal of Software Engineering and Knowledge Engineering*, 29(11n12):1727–1740, 2019.

Appendix

A Applications

The proposed framework is applicable to any spatial machine learning problem where values are predicted for a set of locations. OT should be included in the model evaluation whenever the spatial *displacement* of the predictions plays a role; i.e., when the spatial distribution of the errors has real-world implications. The exact application of OT varies depending on the prediction problem. In this section, we expand on the applications listed in [Table 1](#). Specifically, we outline the applicability of OT by distinguishing three kinds of applications: vision-based GeoAI (essentially segmentation of raster data), point-data time series analysis, and spatial interpolation problems.

A.1 Vision-based GeoAI

Machine learning is used in many geospatial applications, but has arguably brought the most significant advances to problems involving *raster* data. The raster format allows to leverage Convolutional Neural Networks (CNNs) that were developed for image processing but also show impressive performance in classifying, segmenting or regressing geographical raster data. Examples include the analysis of remote sensing data, e.g., for land use classification [\[2\]](#) or for glacier retreat prediction, but also weather forecasting [\[48\]](#) or for predicting sociodemographics in rasterized population data. In remote sensing applications, the spatial distribution of the prediction errors oftentimes plays an important role,

for instance in the locality of weather phenomena or the extend of wildfire spread [79, 82]. Relocating resources, e.g. for extinguishing fire, costs valuable time. OT can quantify such negative effects of prediction errors.

For raster data, the locations l_i correspond to the raster cells or pixels, and the cost matrix C to the pairwise pixel distances, or the operational costs to relocate resources from one pixel to another. For instance, consider the problem of predicting wildfire spread by classifying pixels as “fire” or “no fire”. With the proposed framework, the locations of predicted “fire” pixels can be compared to the true fire extent by means of optimal transport plans. The OT error is higher if the wildfire spreads into an entirely different direction than expected. In contrast, standard accuracy metrics only depend on the pixel counts and do not reflect spatial properties.

A.2 Point-data time series

The focus of this paper is on spatio-temporal prediction problems where the aim is to predict the future observations at given locations. Examples are abundant in the transportation field, for instance including research on bike sharing demand [93, 42, 113, 78, 62, 57], one-way car sharing flow [117], e-scooter fleet utilization [1] or generally shared services [109]. In these fields, ML models are applied to predict transport demand at multiple stations, with the goal of improving efficiency.

The OT error allows to quantify the model’s ability to predict the spatial demand distribution in an interpretable manner. For instance, assume the demand at location a is underestimated while it is overestimated at b . In the OT framework, this leads to a positive value in the OT plan, e.g. $T_{b,a} > 0$. The transport of mass in T can be interpreted as users having to walk from station a to station b to pick up a bike, since the demand at a was underestimated and an insufficient number of bikes is available there. In another interpretation, the flow can be seen as the number of bikes that need to be relocated from b to a at the end of the day to balance out the bike availability. It is worth noting that the business costs of operations in a shared system are far more complex; however, the OT metric adds a spatial aspect to the model evaluation, yielding a better estimate of business costs than non-spatial (standard) error metrics.

However, OT is not restricted to applications that entail relocation operations. For example, consider energy demand prediction, an important research direction in light of the challenging integration of renewable energies. Power system operations and the adoption of electric vehicles (EV) can be supported by predicting the occupancy rate of EV charging stations. The occupancy is the number of plugs at the station that are currently in use. Predictions are relevant for navigating vehicles to the closest stations with available plugs. In turn, prediction errors translate to relocation costs for EV drivers who find a charger unexpectedly occupied. The OT cost thus reflects that real-world costs for drivers are higher the further away the next available station is.

Last, another example is traffic forecasting, a popular branch in GeoAI. Traffic forecasts are relevant for operating signals and for navigation purposes. Prediction errors of traffic forecasting models are more severe if the spatial distribution of traffic is not estimated correctly; i.e., if traffic is expected far from the location where it actually occurs. Thus, OT is useful as a spatial metric in traffic forecasting even though it is not directly interpretable in terms of operational costs. In particular, OT-based evaluation can yield insights into the actual advantages of novel model architectures that are being proposed as spatially-explicit neural networks.

A.3 Spatial interpolation and regression

OT can also be applied to regression problems without a temporal component, for example, inferring housing prices from features such as the property size and its proximity to the city center, or predicting deforestation risks in the rain forest from covariates such as sociodemographics, spatial features, and economic information. In this case, the framework introduced in section 2 can be applied in the same manner as for spatio-temporal time series, since the OT error is computed per time step in any case.

B Geospatial OT for unpaired location sets

In section 2, we limited ourselves to GeoAI applications where the predicted observations are values at the same locations as the ground truth observations. However, this framework is extensible to ML problems that aim to predict *where* an event occurs, instead of predicting the observation at a fixed point. For instance, one could aim to predict the spatial distribution of free-floating car sharing pickups within the next hours to plan car allocations. In this case, the location sets of ground truth and predictions are *unpaired*; i.e., we cannot directly match true with predicted observations.

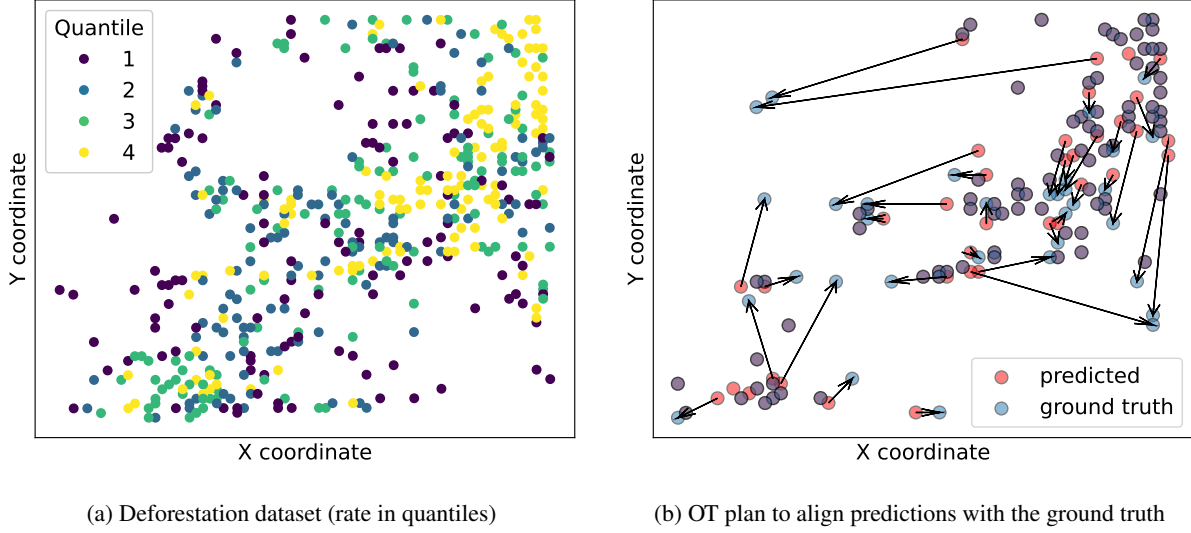


Figure 12: Predicting the location of severe deforestation in the Amazon rainforest. The labels are provided as four quantiles of deforestation rates (a). The predictive model is evaluated in terms of its ability to predict the spatial distribution of the 4th quantile (b). The arrows show the optimal transportation plan to align predictions with the ground truth.

We conduct a case study on this setting, using predictions of where high deforestation will occur. We use a public dataset of deforestation rates to demonstrate how OT can be applied to assess the performance model performance in this task. When implementing policies and designing intervention measures against deforestation, such as information campaigns or financial support for local residents, the spatial locations of the predicted deforestation rates and the distribution of the errors matter. If there is progressive deforestation in regions that are far from the places where it was expected, local campaigns and other measures will not reach the correct regions.

To illustrate the application of OT for a spatial interpolation problem, we train a Random Forest classifier on a dataset published by Santos et al. [85]. It provides the deforestation rates at 2418 locations in the northern Ecuadorian Amazon, given as four classes corresponding to the quantiles of deforestation rates, as well as 35 independent variables covering sociodemographics, land use and population measures. The classifier is trained to predict the deforestation-rate-quantile from the 35 covariates, where 20% of the data are reserved as the test set. The test set is visualized in Figure 12a.

Given the goal of identifying sites for intervention measures, we focus on evaluating the classification performance for the highest quantile. According to standard metrics, the classifier achieves a recall of 0.72 and a precision of 0.7 in detecting high deforestation. Optimal Transport, on the other hand, allows to quantify the correctness of the predicted *spatial* distribution³. Figure 12b visualizes the true and predicted locations of high deforestation rates (i.e., the 4-th quantile), together with the optimal transportation plan T (arrows), computed with partial OT. The OT error E_{POT} corresponds to the total length of the arrows, representing the required re-distribution of mass to match the predicted distribution with the ground truth. Figure 12b shows that the required relocation effort is low in general, with some exceptions such as unpredictably high deforestation rates in the upper left. Thus, OT-based evaluation provides a more fine-grained and informative assessment of predictive models than the classification accuracy.

C Data and preprocessing

The bike sharing dataset was downloaded from Kaggle⁴ and restricted to the period from 15th of April to 15th of November 2014, since the service is closed in winter, leading to large gaps in the time series across years. Only stations with missing coordinates or maintenance stations were removed.

³Contrary to our simplified explanation of spatio-temporal OT in section 2, the locations of the true and predicted observations do not have to be identical. In this context, the cost matrix is calculated as the Euclidean distance between two distinct sets of locations, with the masses P and Q represented as uniform distributions

⁴<https://www.kaggle.com/datasets/aubertsigouin/biximt1>

The charging station occupancy dataset was published by Amara-Ouali et al. [3] in the context of the “Smarter Mobility Data Challenge”. Each charging station has three plugs and the challenge is to classify the state of each plug as “available”, “charging”, “passive” (plug is connected to a car that is fully charged) and “other” (out of order). Here, we frame the task as a regression problem of predicting the fraction of plugs that are occupied, i.e., *charging* or *passive*. The forecasts could help to estimate the energy demand and to facilitate planning of charging stops for owners of electric vehicles.

The data is given at a granularity of 15 minutes from 3rd of July 2020 to 18th of February 2021. The time series is comparably sparse, since a station on average has no plugs in use 61% of the time; one out of three plugs in use by 27%, and only 2.1% where all three plugs are used. From 2020-10-22 onwards, there is also a considerable number of missing data, amounting to 8% of missing information on the number of chargers in use. We execute the preprocessing pipeline⁵ of the winning team of the “Smarter Mobility Data Challenge”, who employ exponential moving weighted average to fill missing values. We further removed stations with no charging activity, leaving 83 charging stations. Finally, we scale all values by dividing by 3 for training the model.

The PEMS traffic dataset is published by the California Department of Transportation⁶ and was downloaded from GitHub⁷ where it was published by Guo et al. [37]. It provides traffic flow, traffic occupancy rate, and traffic speed at each sensors in five minute intervals for 62 days (July to August in 2016). We predict only traffic flow. Furthermore, there data includes the spatial distances between certain pairs of sensors. We construct the cost matrix by computing the all-pairs shortest paths in an undirected graph that was built from the given distances.

D Model training

In all cases, we train an established time series prediction model, N-HiTS [13], implemented in the *darts* library [39]. The model was chosen since it outperformed other common approaches such as Exponential Smoothing, LightGBM [50] or XGBoost in our initial experiments.

The model is trained for 100 epochs with early stopping. The learning rate was set to $1e^{-5}$. The time series was treated as multivariate data with one variable per bike sharing station or charging station. A lag of 24 is used to learn daily patterns, and the hour and weekday are provided as past covariates. The number of stacks in the N-HiTS model was set to 3. The number of output time steps corresponds to our forecast horizon of five time steps. For evaluation, we draw 100 samples from the test data (last 10% of the time series) and predict the next five time steps based on the respectively preceding time series, without re-training the model. For further implementation details, we refer to our source code.

E Partial OT as a combination of distributional and total costs

Intuitively, partial OT strikes a balance between balanced OT (measuring the mismatch between the predicted and true distribution) and the total error δ (mismatch between the sum of predicted and the sum of observed values). The weighting between both depends on ϕ . In Table 3, we reported the results for the partial OT error with low ϕ , specifically setting ϕ to the 0.1-quantile of all pairwise costs C_{ij} , and high ϕ , where ϕ is set to the maximum of the cost matrix $\phi = \max_{ij} C_{ij}$. The reasoning of these parameter settings is illustrated in Figure 13, showing the OT error of the model trained on predicting charging data occupancy with a Sinkhorn loss. In particular, Figure 13 illustrates the dependence of E_{POT} on ϕ . For ensuring comparability of E_{OT} and E_{POT} , the extended cost matrix \tilde{C} was normalized by its maximum for this illustration.

We observe that the E_{POT} approximately corresponds to E_{OT} when ϕ is set to the 0.1-quantile of C (intersection of green and blue lines in Figure 13). This observation is consistent for synthetic data as well as the bike sharing dataset. The reason is that with $\phi = 0$, only the spatial distribution would be penalized, but some mass could be imported to / exported from arbitrary locations for free. Thus, $\phi = 0$ leads to lower errors than E_{OT} .

On the other hand, for $\phi \rightarrow \infty$, all entries of C become zero except for the last row and column which is 1, since all values are divided by ϕ when normalizing by the maximum.

Thus, E_{POT} converges to δ for large ϕ (blue line approaching red line). When $\phi = \max_{ij} C_{ij}$, the partial OT error is maximal since E_{OT} is combined with δ .

⁵Available on GitHub:<https://github.com/arthur-75/Smarter-Mobility-Data-Challenge>

⁶<https://pems.dot.ca.gov>

⁷<https://github.com/guoshnBJTU/ASTGNN/tree/main/data/PEMS08>

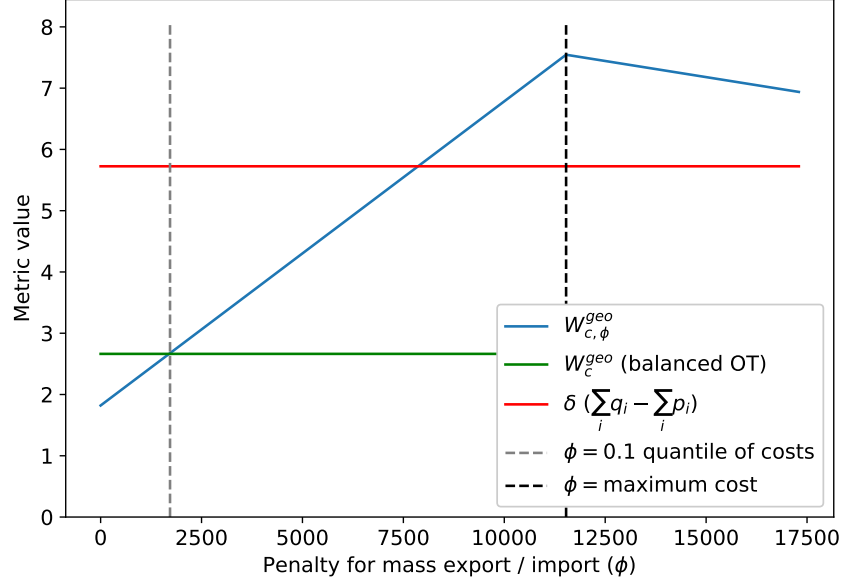


Figure 13: Relation of E_{POT} to ϕ in one synthetic example

F Comparison of spatial aggregation scales with normalized errors

The comparability of predictions of different cluster sizes with the MSE could be improved by computing the average error per station, formally $MSE_{normed}(Y, \hat{Y}) = \sum_{G \in \mathcal{G}} \sum_{i \in G} (\frac{y_i - \hat{y}_i}{|G|})^2$, where \mathcal{G} is the set of all clusters and G is one cluster. Figure 14 demonstrates that for our bike sharing demand prediction task, MSE_{normed} increases with the granularity, since the data for one station is more noisy and harder to predict.

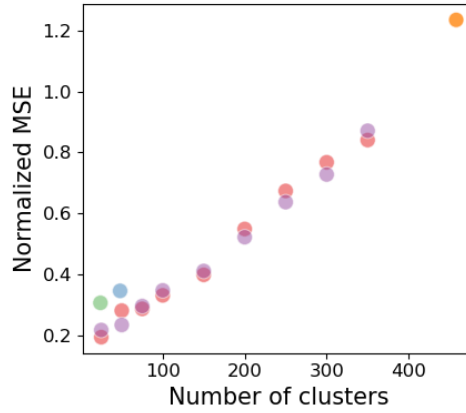


Figure 14: Normalized MSE by clustering scheme. The demand at larger clusters is easier to predict due to a better signal-to-noise ratio